Achievable Rate Analysis of Two-Hop Interference Channel with Coordinated IRS Relay

The Vi Nguyen, Thanh Phung Truong, Thi My Tuyen Nguyen, Wonjong Noh, *Senior Member, IEEE*, and Sungrae Cho, *Member, IEEE*

***Abstract*—Intelligent reflecting surface (IRS) is a promising 6G technology that can improve wireless communication capacity in a cost-effective and energy-efficient manner, by adjusting a large number of passive reflectors to appropriately change the signal propagation. In this study, we identified the achievable rate region of a two-hop interference channel with distributed multiple IRS relays. To do so, we formulated a non-convex problem that characterizes the rate-profile, and found its solution using successive convex approximation (SCA). We then proposed an alternating direction method of multipliers (ADMM) and alternating optimization (AO) based distributed and low-complex IRS control that maximizes the achievable sum-rate, and proved its convergence and optimality. We then compared the proposed IRS control with semi-definite relaxation (SDR)-, random phase-, deep reinforcement learning (DRL)- based IRS controls, and optimal amplify-and-forward (AF)-, interference neutralization (IN)-, and decode-and-forward (DF) based relaying schemes. We demonstrated that the proposed control with multiple IRS elements outperforms the benchmark controls in terms of the achievable rate region, achievable sum-rate, and energy efficiency under same power budget. We also confirmed that the discrete phase approximation of the proposed control provides near-optimal performance with fewer bits, and the proposed control is robust under imperfect CSI condition. The proposed controls can be efficiently applied to large-scale multi-pair multihop device-to-device and machine-type device communications in the interference-limited or low-powered dense networks of 5G and 6G environments.**

***Index Terms*—Coordinated relay, intelligent reflecting surface, interference channel, multihop multi-pair transmission**

I. Introduction

THE unprecedented demands for high quality and ubiquitous wireless services impose enormous challenges to existing cellular networks. Applications such as rate-centric enhanced mobile broadband (eMBB), ultra-reliable and low-latency communications (URLLC), and massive machine type communications (mMTC) services are the targets for the design of fifth-generation (5G) communication systems. However, the goals of sixth-generation (6G) wireless communication systems are expected to be transformative and revolutionary encompassing applications such as data-driven, instantaneous, ultra-massive, and ubiquitous wireless connectivity, as well as connected intelligence [1]. To achieve this goal, an intelligent reflecting surface (IRS) and its various equivalents have emerged as a new and promising solution. The advantages of an IRS are as follows [1]. First, such a surface can easily be applied to building facades, indoor walls, aerial platforms, roadside billboards, highway polls, and vehicle windows. Second, an enhanced spectral efficiency enhancement is provided by forming line-of-sight (LoS) links between base stations (BSs) and mobile users and enhancing the received signal-to-interference-plus-noise ratio (SINR). It is also more energy-efficient and environment-friendly than conventional amplify-and-forward (AF) and decode-and-forward (DF) systems. Third, it can operate in a full-duplex (FD) and full-band transmission without requiring additional power for signal amplification/regeneration as well as a sophisticated processing for self-interference cancellation. Finally, it can be densely deployed in wireless networks at low cost and with a low energy consumption because it mainly constitutes passive devices without the need for active transmit RF chains.

There have been many recent studies on IRSs. Some initial efforts have been focused on employing IRSs for realizing smart radio environments in wireless networks: IRS prototype, holographic multiple-input multiple-output (MIMO) surfaces [2], [3], hardware architectures [4], [5], electromagnetic-based communication-theoretic framework for analyzing and optimizing metamaterial-based IRSs [4], and several application scenarios under different assumptions [6], [7]. However, new challenges keep arising in the design and implementation of IRS-aided wireless systems. Moreover, there is an insufficient number of studies on optimal IRS control in IRS-assisted multihop networks.

A. Related Work

1) IRS in single-hop single-pair transmission: Many studies [8]–[14] have focused on IRS-assisted point-to-point communications. J. Zhang *et al.* [8] studied a statistically robust beamforming design for an IRS-assisted multiple-input single-output (MISO) wireless system under imperfect channel state information (CSI). This design aims at jointly optimizing the transmit/receive beamformers and IRS phase shifts to minimize the average mean squared error (MSE) at the user side. H. Guo *et al.* [10] proposed a discrete IRS phase control approach for an IRS-aided multiuser MISO system. It maximizes the weighted sum-rate by jointly optimizing the

This work was supported by the National Research Foundation of Korea (NRF) grant funded by the Korea government (MSIT) (NRF-2019R1A2C1090447 and 2020R1F1A1069119), and the Chung-Ang University Young Scientist Scholarship in 2021. *(Corresponding authors: Wonjong Noh and Sungrae Cho.)*

T. V. Nguyen, T. P. Truong, T. M. T. Nguyen, and S. Cho are with the School of Computer Science and Engineering, Chung-Ang University, Seoul 156-756, South Korea (e-mail: tvnguyen@uclab.re.kr, tptruong@uclab.re.kr, tuyen@uclab.re.kr, srcho@cau.ac.kr).

W. Noh is with the School of Software, Hallym University, Chuncheon 24252, South Korea (e-mail: wonjong.noh@hallym.ac.kr).

active beamforming at the base-station (BS) and the passive beamforming at the IRS. In addition, S. Zhang *et al.* [11] and N. Perovic *et al.* [12] characterized the fundamental capacity limit and achievable rate of IRS-aided MIMO communication systems by jointly optimizing the IRS reflection coefficients and the MIMO transmit covariance matrix. Q. Wu *et al.* [9] and Z. Yang *et al.* [13] proposed low-complexity distributed algorithms where the access point (AP) and IRS independently adjust the transmit beamforming and phase shifts in an alternating manner. In [9], the total received signal power at the user side is maximized, whereas in [13], the energy efficiency of the network is maximized by dynamically controlling the on-off status of each IRS as well as optimizing the reflection coefficient matrix of the IRSs.

2) IRS in single-hop multi-pair transmission: Some studies [15]–[19] have considered the achievable rates in an IRS-assisted multi-pair source-destination model with direct source-to-destination channel. W. Huang *et al.* [15] investigated the achievable rate region of an IRS-assisted MISO interference channel, which exploits the additional design degree-of-freedom (DoF) provided by the coordinated IRSs to enhance the desired signal and to suppress interference, thereby enlarging the achievable rate region of the interference channel. To address the non-convex optimization problem, an iterative algorithm was proposed to optimize the transmit beamforming through the second-order cone program (SOCP), and reflective beamforming through the semi-definite relaxation (SDR). Z. Zhang *et al.* [16] proposed the concept of an IRS-aided cell-free network to improve the network capacity with low cost and power consumption. Then, for the proposed IRS-aided cell-free network in a typical wideband scenario, a joint precoding design problem at the BSs and RISs is formulated to maximize the network capacity. Owing to the non-convexity and high complexity of the formulated problem, an alternating optimization algorithm is developed to solve this challenging problem. Simulation results verify that, compared with the conventional cell-free network, the network capacity of the proposed scheme can be significantly improved. S. Huang *et al.* [17] proposed a fully decentralized cooperative beamforming in IRS-aided cell-free networks. It first transforms the centralized weighted sum-rate maximization problem into a tractable consensus optimization problem, and an incremental ADMM algorithm is proposed to locally update the beamformer. M. Hua *et al.* [18] proposed an IRS-assisted joint processing coordinated multipoint (JP-CoMP) transmission from multiple BSs to multiple cell-edge users. By considering the fairness among cell-edge users, the authors aim at maximizing the minimum achievable rate of such users. Furthermore, the proposed JP-CoMP design significantly outperforms the conventional coordinated scheduling/coordinated beamforming coordinated multipoint (CS/CB-CoMP) design in terms of the max-min rate. A. Bafghi *et al.* [19] studied the DoF of the time-selective K-user interference channel in the presence of an IRS. It is well known that the sum DoF of the time-selective K-user interference channel without IRS is $K/2$. However, it shows that an IRS-assisted K-user interference channel is able to enlarge the DoF region and provide the full K sum DoF, when the number of IRS elements is sufficiently large.

3) IRS in multi-hop transmission: The direct communication links may be blocked by both thick walls in indoor scenarios and trees and large buildings in outdoor scenarios, particularly in high-frequency millimeter-wave communication systems. Some studies [20]–[24] considered the achievable rates in an IRS-assisted source-destination model with indirect source-to-destination channel. In particular, Z. Peng *et al.* [20] derived the achievable rate of the IRS-assisted single-antenna transmitter and receiver system when considering the statistical CSI, which is easier to obtain because it varies more slowly. Using a genetic algorithm (GA) method, continuous and discrete phase shift optimization problems were solved. Assuming that one of multiple IRSs is selected to aid in the communication process, L. Yang *et al.* [21] presented an exact analysis for the outage probability, closed-form expressions for the asymptotic outage probability, the asymptotic sum-rate, and the capacity scaling law. H. Du *et al.* [22] proposed RIS-aided and AF relay systems, which consider the fluctuating two-ray (FTR) distribution to model the small-scale fading within the mmWave frequency, whereas previous works used Rayleigh or Rician fading. J. He *et al.* [23] proposed a distributed IRS-empowered communication network architecture, where multiple source destination pairs communicate through distributed multiple IRSs. With this architecture, a fractional programming based alternating approach to maximize the achievable sum-rates was developed. In particular, the closed-form expressions are proposed for coordinated passive beamforming at the IRSs. M. Zeng *et al.* [24] studied the resource allocation for an IRS-assisted uplink system, where the BS is equipped with multiple antennas. In this case, a joint optimization of the transmit power of the users, active beamforming at the base station, and passive beamforming at the IRS are proposed to maximize the overall system energy efficiency while maintaining the minimum rate constraints of the users.

B. Motivation, Contribution, and Organization

IRS-aided multi-pair communication systems have recently become a typical communication approach owing to the rapid increase in the number of machine-type devices in future networks. This work considers two-hop IRS-assisted relaying networks with multiple single-antenna source-destination pairs communicating through distributed multiple IRS modules, which has yet to be sufficiently studied. Our main contributions can be summarized as follows:

- We identified the achievable rate region of a two-hop interference channel with distributed and cooperative IRS relays. To do this, we formulated a non-convex problem that characterizes the rate-profile and found its solution using successive convex approximation (SCA).
- We identified maximum achievable sum-rate. For this, we also proposed an alternating optimization (AO) and alternating direction method of multipliers (ADMM) based distributed IRS control and proved rigorously the solution's convergence and optimality.

- We analyzed that the proposed IRS control has polynomial computation complexity and has lower complexity than other conventional comparing schemes.
- We demonstrated that the proposed IRS control provides an enhanced system performance when compared with semi-definite relaxation (SDR)-, random phase-, deep reinforcement learning (DRL)-based IRS controls, and optimal amplify-and-forward (AF)-, interference neutralization (IN)-, decode-and-forward (DF)-based relaying schemes, in terms of the achievable rate region, achievable sum-rate, and energy efficiency under same power budget. We also confirmed that the discrete phase approximation of the proposed control provides near-optimal performance with 3-bit quantizations, and the proposed control provides robust performance under imperfect CSI condition.
- The proposed control can be efficiently applied to large-scale multi-pair multihop device-to-device (D2D) and machine-type device communications in interference-limited or low-powered dense networks.

The rest of this paper is organized as follows. In Section II, we introduce the system model. In Section III, we characterize the achievable rate region and find the maximal sum rate for a coordinated IRS system. In Section IV, numerical results are provided to demonstrate the correctness of our analysis. Conclusions are presented in Section V.

Notations: We denote the scalar quantities in lowercase letters (e.g., x), vector quantities in lowercase boldface letters (e.g., $\boldsymbol{x}$), and matrix quantities in capital boldface letters (e.g., $\boldsymbol{X}$). The operators $(\cdot)^T$ and $(\cdot)^*$ denote the transpose and complex conjugate, respectively. $\mathbb{C}$ and $\mathbb{C}^{M\times N}$ denote the space of complex numbers and space of M-by-N complex matrices, respectively. For a complex number x, $|x|$ represents the modulus of x; $\arg(x), Re(x)$, and $Im(x)$ represent the argument, real, and imaginary parts of x, respectively; and $j=\sqrt{-1}$ is the complex imaginary unit. For a vector $\boldsymbol{x}$, $\|\boldsymbol{x}\|_2$ denotes the Euclidean norm of $\boldsymbol{x}$; and diag$\{x_1,...,x_n\}$ denotes an $n\times n$ diagonal matrix, whose each diagonal entry is x_i. For a matrix $\boldsymbol{A}$, the notations $\boldsymbol{A}^H, \boldsymbol{A}^*$, and $\boldsymbol{A}^\star$ represent the conjugate transpose, complex conjugate, and converged solution, respectively; tr$(\boldsymbol{A})$ represents the trace of $\boldsymbol{A}$ (if $\boldsymbol{A}$ is a square matrix); and vec$(\boldsymbol{A})$ represents a vector obtained by stacking the columns of $\boldsymbol{A}$. For two matrices $\boldsymbol{A}$ and $\boldsymbol{B}$, $\boldsymbol{A}*\boldsymbol{B}$ and $\boldsymbol{A}\otimes\boldsymbol{B}$ represent the Khatri-Rao and Kronecker products, respectively. In addition, $\boldsymbol{I}_N$ denotes an N-by-N identity matrix, $\iota_{\mathcal{F}}(\cdot)$ denotes the projection onto set $\mathcal{F}$, and $\mathcal{CN}(\boldsymbol{\mu},\boldsymbol{\Sigma})$ denotes the circularly symetric complex Gaussian (CSCG) distribution of a random complex vector with mean vector $\boldsymbol{\mu}$ and covariance matrix $\boldsymbol{\Sigma}$.

II. System Model: Two-hop Interference Channel with Multiple IRS Relays

In this study, we focused on two-hop multiple IRS based relaying system. In the relaying system, the direct communication links may be blocked by both thick walls in indoor scenarios and trees and large buildings in outdoor scenarios, particularly in high-frequency millimeter-wave communication systems. Here, the IRS can be easily installed at the desired location as needed. Therefore, we assume there is no direct path between sources and destinations. As shown in Fig. 1, a two-hop interference channel with L IRSs is considered to aid the communication between K pairs of sources and destinations. Each pair is indexed by $k\in\mathcal{K}\triangleq\{1,2,...,K\}$. For $k\in\mathcal{K}$, both the k-th source and its destination are equipped with one antenna. Each IRS is indexed by $i\in\mathcal{L}\triangleq\{1,2,...,L\}$. For $i\in\mathcal{L}$, the i-th IRS has M_i reflecting elements. For the distributed multiple IRS, we also assume one central controller which is deployed to coordinate the operation of all IRSs. Each IRS module updates its local phase shift and the central controller aggregates local phase shifts. Here, the global phase aggregation can be efficiently computed using the recent over-the-air-computation (AirComp) technique [25].

A. Channel Model

We denote $\boldsymbol{e}_{i,k}\in\mathbb{C}^{M_i\times 1}$ to be the channel-coefficient vector from the k-th source to the i-th IRS, and $\boldsymbol{E}_i\triangleq[\boldsymbol{e}_{i,1},...,\boldsymbol{e}_{i,K}]\in\mathbb{C}^{M_i\times K}$ to be the matrix that composes these vectors. Let $\boldsymbol{f}_{k,i}\in\mathbb{C}^{M_i\times 1}$ denote the channel coefficient vector between the i-th IRS and the k-th destination. In this work, we assume that the channels experience a *block fading* and *flat fading*. Also, we assume perfect channel state information (CSI). In practice, the IRSs are deployed on the facade of a buiding, which are close to the users, therefore we can assume that the *line-of-sight* path exists in the source-IRS links and IRS-destination links. Thus, the channel $\boldsymbol{e}_{i,k}$ can be modeled as a Rician fading channel as follows:

$$\boldsymbol{e}_{i,k}=\sqrt{\eta(d_{i,k})}\left(\sqrt{\frac{\kappa_1}{1+\kappa_1}}\boldsymbol{e}_{i,k}^{\text{LoS}}+\sqrt{\frac{1}{1+\kappa_1}}\boldsymbol{e}_{i,k}^{\text{NLoS}}\right), \quad (1)$$

where $\eta(d_{i,k})$ is the large-scale path loss component of the channel that depends on the distance $d_{i,k}$ between the k-th source and i-th IRS; $(\boldsymbol{e}_{i,k}^{\text{LoS}}\ ,\ \boldsymbol{e}_{i,k}^{\text{NLoS}})$ is the small-scale component including LoS and NLoS components, respectively, and κ_1 is the Rician factor. Elements of the NLoS component are i.i.d and follow the complex Gaussian distribution with zero mean and unit variance. For the LoS components, we consider that each IRS has uniform rectangular array (URA), then the LoS component $\boldsymbol{e}_{i,k}^{\text{LoS}}$ can be modeled as follows [26]:

$$\boldsymbol{e}_{i,k}^{\text{LoS}}=\boldsymbol{a}\left(\alpha_{i,k}^{\text{AoA}},\beta_{i,k}^{\text{AoA}}\right), \quad (2)$$

where $\alpha_{i,k}^{\text{AoA}}$ and $\beta_{i,k}^{\text{AoA}}$ are the azimuth angle of arrival (AoA) and elevation AoA, respectively, at the i-th IRS from the k-th source; $\boldsymbol{a}\left(\alpha_{i,k}^{\text{AoA}},\beta_{i,k}^{\text{AoA}}\right)$ is the steering vector, which is expressed as:

$$\boldsymbol{a}\left(\alpha_{i,k}^{\text{AoA}},\beta_{i,k}^{\text{AoA}}\right)=\boldsymbol{a}_v\left(\alpha_{i,k}^{\text{AoA}},\beta_{i,k}^{\text{AoA}}\right)\otimes\boldsymbol{a}_h\left(\alpha_{i,k}^{\text{AoA}},\beta_{i,k}^{\text{AoA}}\right)\in\mathbb{C}^{M_i\times 1}, \quad (3)$$

where $\boldsymbol{a}_v\left(\alpha_{i,k}^{\text{AoA}},\beta_{i,k}^{\text{AoA}}\right)\in\mathbb{C}^{M_i^v\times 1}$ and $\boldsymbol{a}_h\left(\alpha_{i,k}^{\text{AoA}},\beta_{i,k}^{\text{AoA}}\right)\in\mathbb{C}^{M_i^h\times 1}$ represent the steering vector in the vertical and horizontal directions, respectively. Here, M_i^v and M_i^h denote the number of IRS elements along the vertical and horizontal

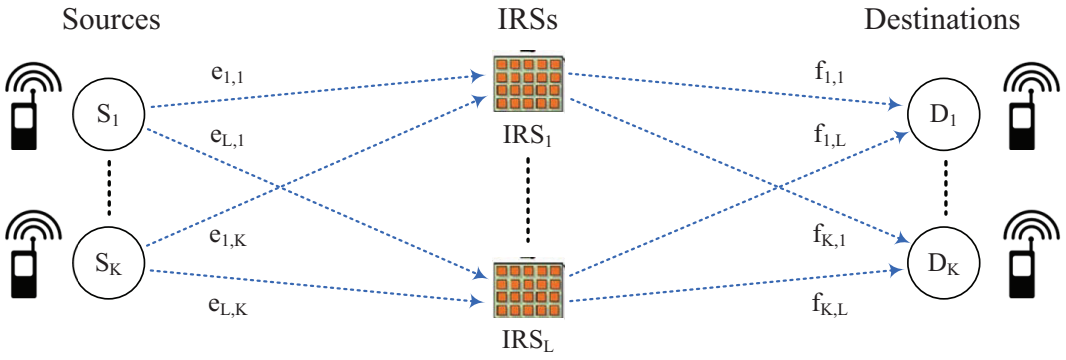

Fig. 1. RIS-aided Multihop Multi-Pair Unicast Network

axes, respectively. Accordingly, each element of these vectors are modeled as follows [26]:

$$\left[\boldsymbol{a}_v\left(\alpha_{i,k}^{\text{AoA}},\beta_{i,k}^{\text{AoA}}\right)\right]_{n_1} = e^{j\frac{2\pi d}{\lambda}(n_1-1)\cos(\beta_{i,k}^{\text{AoA}})\cos(\alpha_{i,k}^{\text{AoA}})}, \quad \forall n_1 \in \{1,2,...,M_i^v\}, \tag{4}$$

$$\left[\boldsymbol{a}_h\left(\alpha_{i,k}^{\text{AoA}},\beta_{i,k}^{\text{AoA}}\right)\right]_{n_2} = e^{-j\frac{2\pi d}{\lambda}(n_2-1)\cos(\beta_{i,k}^{\text{AoA}})\sin(\alpha_{i,k}^{\text{AoA}})}, \quad \forall n_2 \in \{1,2,...,M_i^h\}, \tag{5}$$

where d and λ are the distance between the adjacent IRS elements and carrier wavelength. For simplicity, we set $d/\lambda = 1/2$. Similarly, the channel $\boldsymbol{f}_{k,i}$ can be modeled as follows:

$$\boldsymbol{f}_{k,i} = \sqrt{\eta(\tilde{d}_{k,i})}\left(\sqrt{\frac{\kappa_2}{1+\kappa_2}}\boldsymbol{f}_{k,i}^{\text{LoS}} + \sqrt{\frac{1}{1+\kappa_2}}\boldsymbol{f}_{k,i}^{\text{NLoS}}\right), \tag{6}$$

where $\eta(\tilde{d}_{k,i})$ is the large-scale path loss component and $\tilde{d}_{k,i}$ is the distance between the i-th IRS and k-th destination; κ_2 is the Rician factor; $\boldsymbol{f}_{k,i}^{\text{NLoS}}$ are the NLoS components, whose elements are i.i.d and follow the complex Gaussian distribution with zero mean and unit variance; $\boldsymbol{f}_{k,i}^{\text{LoS}}$ are the LoS components, and $\boldsymbol{f}_{k,i}^{\text{LoS}} = \boldsymbol{a}\left(\alpha_{k,i}^{\text{AoD}},\beta_{k,i}^{\text{AoD}}\right)$, where $(\alpha_{k,i}^{\text{AoD}},\beta_{k,i}^{\text{AoD}})$ are the azimuth angle of departure (AoD) and elevation AoD from the i-th IRS to the k-th destination, respectively.

B. Discussion on Channel Estimation

In this work, in order to find the optimal phase shift, the IRS-relay system requires accurate channel state information including source-IRS, i.e., $\{\boldsymbol{e}_{i,k}\}$ and IRS-destination channel vectors, i.e., $\{\boldsymbol{f}_{k,i}\}$. Archiving high-accurate CSI is a challenge, due to the high dimension of those channel vectors with large number of IRS elements. In addition, all IRS elements are passive, which is not capable of signal processing, so it is difficult to realize the channel estimation. However, some recent practical channel estimation and acquisition techniques can be used for obtaining the perfect CSI, such as the brute-force method in [27], the discrete Fourier transform (DFT)-matrix quantization in [28], the compressed sensing method in [29], the efficient CSI acquisition method for RIS-aided mmWave network [30], the fast channel estimation [31], and the transforming fast fading channel to slow fading channel [32]. With the help of those works, we assumed perfect CSI and slow fading. In fact, the performance with perfect CSI can be treated as an upper bound of the performance in the real IRS networks.

C. Signal Model

Let s_k denote the transmit symbol from the k-th source, for $k \in \mathcal{K}$. The transmit symbols are assumed to be independent and identically distributed (i.i.d.) CSCG random variables with zero mean and unit variance, i.e., $\mathbb{E}[s_k s_{\tilde{k}}^*] = 0$, for $k \neq \tilde{k}$ and $s_k \sim \mathcal{CN}(0,1), \forall k \in \mathcal{K}$. Denote $\boldsymbol{s} \triangleq [s_1,...,s_K]^T \in \mathbb{C}^{K\times 1}$ as the vector of the transmit symbols from all sources in $\mathcal{K}$. We assume that the IRSs can operate in FD mode with AF protocol without self-interference. Hence, the received signal at the k-th destination is written as

$$y_k = \underbrace{\sum_{i=1}^{L}\sqrt{p_k}\boldsymbol{f}_{k,i}^T\boldsymbol{\Phi}_i\boldsymbol{e}_{i,k}s_k}_{\text{Desired signal } (y_{S,k})} + \underbrace{\sum_{i=1}^{L}\boldsymbol{f}_{k,i}^T\boldsymbol{\Phi}_i\bar{\boldsymbol{E}}_{i,k}\bar{\boldsymbol{P}}_k^{\frac{1}{2}}\bar{\boldsymbol{s}}_k}_{\text{Interference signal } (y_{I,k})} + n_k, \tag{7}$$

where $\boldsymbol{\Phi}_i \triangleq \text{diag}\{e^{j\theta_{i,1}},...,e^{j\theta_{i,M_i}}\} \in \mathbb{C}^{M_i\times M_i}$ is the reflection-coefficient matrix of the i-th IRS, and $\theta_{i,m}$ is the phase shift of the m-th element of the i-th IRS. For each $m \in \{1,...,M_i\}$, applying the change in variable $\phi_{i,m} = e^{j\theta_{i,m}}$ yields $\boldsymbol{\Phi}_i = \text{diag}\{\phi_{i,1},...,\phi_{i,M_i}\}$. We denote $\boldsymbol{\phi}_i \triangleq [\phi_{i,1},...,\phi_{i,M_i}]^T \in \mathbb{C}^{M_i\times 1}$ as the collection of diagonal entries of the matrix $\boldsymbol{\Phi}_i$, n_k is the additive noise at the k-th destination with distribution $\mathcal{CN}(0,\sigma_d^2)$, $\bar{\boldsymbol{s}}_k \triangleq [s_1,\ldots,s_{k-1},s_{k+1},\ldots,s_K]^T \in \mathbb{C}^{(K-1)\times 1}$, $\bar{\boldsymbol{P}}_k \triangleq \text{diag}\{p_1,\ldots,p_{k-1},p_{k+1},\ldots,p_K\} \in \mathbb{C}^{(K-1)\times(K-1)}$, and $\bar{\boldsymbol{E}}_{i,k} \triangleq [\boldsymbol{e}_{i,1},\ldots,\boldsymbol{e}_{i,k-1},\boldsymbol{e}_{i,k+1},\ldots,\boldsymbol{e}_{i,K}] \in \mathbb{C}^{M_i\times(K-1)}$ denote the vector of the transmit symbol targeting destinations excluding the k-th destination, the corresponding power matrix, and the matrix containing vectors of the channel coefficients from the corresponding source to the i-th IRS, respectively. Let $y_{S,k}$ and $y_{I,k}$ be the desired signal and interference signal, respectively. Accordingly, $P_{S,k}$ and $P_{I,k}$ are denoted as the desired signal power and interference signal power at the k-th destination, respectively. They are expressed in the closed forms given in the following proposition.

Proposition 1. *The desired signal power and interference signal power are as follows:*

(a) *The desired signal power is given by*

$$P_{S,k} = \mathbb{E}[|y_{S,k}|^2] = p_k(\boldsymbol{\phi}^H \boldsymbol{S}_k \boldsymbol{\phi}), \tag{8}$$

where $\boldsymbol{\phi} \triangleq \left[\boldsymbol{\phi}_1^T, ..., \boldsymbol{\phi}_L^T\right]^T \in \mathbb{C}^{\sum_{i=1}^L M_i \times 1}$, $\boldsymbol{a}_k \triangleq \left[\left(\boldsymbol{e}_{1,k}^T * \boldsymbol{f}_{k,1}^T\right), \ldots, \left(\boldsymbol{e}_{L,k}^T * \boldsymbol{f}_{k,L}^T\right)\right]^H \in \mathbb{C}^{\sum_{i=1}^L M_i \times 1}$, *and* $\boldsymbol{S}_k \triangleq \boldsymbol{a}_k \boldsymbol{a}_k^H \in \mathbb{C}^{\sum_{i=1}^L M_i \times \sum_{i=1}^L M_i}$.

(b) *The interference signal power is given by*

$$P_{I,k} = \mathbb{E}[|y_{I,k}|^2] = \boldsymbol{\phi}^H \boldsymbol{K}_k \boldsymbol{\phi}, \tag{9}$$

where $\boldsymbol{B}_k \triangleq \left[\left(\bar{\boldsymbol{E}}_{1,k} \bar{\boldsymbol{P}}_k^{\frac{1}{2}}\right)^T * \boldsymbol{f}_{k,1}^T, ..., \left(\bar{\boldsymbol{E}}_{L,k} \bar{\boldsymbol{P}}_k^{\frac{1}{2}}\right)^T * \boldsymbol{f}_{k,L}^T\right] \in \mathbb{C}^{(K-1) \times \sum_{i=1}^L M_i}$, *and* $\boldsymbol{K}_k \triangleq \boldsymbol{B}_k^H \boldsymbol{B}_k \in \mathbb{C}^{\sum_{i=1}^L M_i \times \sum_{i=1}^L M_i}$.

Proof. Please see appendix A. □

From Proposition 1, the SINR at the kth destination in the system is obtained as

$$\text{SINR}_k = \frac{p_k(\boldsymbol{\phi}^H \boldsymbol{S}_k \boldsymbol{\phi})}{\boldsymbol{\phi}^H \boldsymbol{K}_k \boldsymbol{\phi} + \sigma_d^2}. \tag{10}$$

The achievable rate at the k-th destination is given by

$$R_k(\boldsymbol{\phi}) = \log_2(1 + \text{SINR}_k). \tag{11}$$

In the following section, we propose two algorithms for finding the *achievable rate region* and *optimal sum-rate* of the two-hop interference channel with multiple coordinated IRSs.

III. Proposed Algorithms

A. Characterization of Achievable Rate Region

The achievable rate region is defined as the set of rate-tuples that are simultaneously achievable at all destinations under the unit-modulus constraint on the phase shifts at the IRSs. This is defined as follows:

$$\mathcal{R} = \bigcup_{\substack{|\phi_{i,m}|=1 \\ \forall m \in \{1,...,M_i\}, \forall i \in \mathcal{L}}} \left\{(r_1, ..., r_K) : 0 \le r_k \le R_k(\boldsymbol{\phi}), k \in \mathcal{K}\right\}. \tag{12}$$

The outer boundary of $\mathcal{R}$ is called the *Pareto boundary*, which consists of rate-tuples at which it is impossible to increase a certain user's rate without simultaneously decreasing that of other users [33]. Based on the *rate profile* method [33], the rate-tuple on the Pareto boundary is obtained by solving the following problem:

$$\max_{R, \boldsymbol{\phi}} \quad R \tag{13a}$$

$$\text{s.t.} \quad \log_2\left(1 + \text{SINR}_k\right) \ge \mu_k R, \quad \forall k \in \mathcal{K}, \tag{13b}$$

$$|\phi_{i,m}| = 1, \quad \forall m \in \{1, ..., M_i\}, \forall i \in \mathcal{L}, \tag{13c}$$

where the given rate-profile vector $\boldsymbol{\mu} = [\mu_1, ..., \mu_K]^T$ satisfies $\mu_k \ge 0, \forall k \in \mathcal{K}$, and $\sum_{k=1}^K \mu_k = 1$. Here, μ_k specifies the target ratio between the achievable rate of the k-th destination and the sum rate of the destinations, which is denoted as R. More specifically, our achievable rate region problem is as follows:

$$\max_{R, \boldsymbol{\phi}} \quad R \tag{14a}$$

$$\text{s.t.} \quad \log_2\left(1 + \frac{p_k(\boldsymbol{\phi}^H \boldsymbol{S}_k \boldsymbol{\phi})}{\boldsymbol{\phi}^H \boldsymbol{K}_k \boldsymbol{\phi} + \sigma_d^2}\right) \ge \mu_k R, \quad \forall k \in \mathcal{K}, \tag{14b}$$

$$\text{(13c)}. \tag{14c}$$

This problem can be solved by using Gaussian randomization-based semidefinite relaxation (SDR) together with the bi-section method [15]. However, the Gaussian randomization cannot always guarantee to recover the rank-one SDR solution. In addition, the computational complexity raises very high with the large number of IRS elements. To address such issues, we apply the successive convex approximation (SCA) method, which is a method with performance guarantee and lower complexity. Due to the non-convexity of the unit-modulus constraint (13c), the problem can be hard to be solved. To handle such difficulty, we first relax this constraint as $|\phi_{i,m}| \le 1$, for all $m \in \{1, .., M_i\}, i \in \mathcal{L}$, then the unit-modulus solution will be recovered by using the projection. The relaxed problem can be solved as follows. Inspired by [34], we apply SCA method to update $(\boldsymbol{\phi}, R)$ iteratively, which guarantees the achievable rate constraints. In particular, at iteration t, we aim to find $\boldsymbol{\phi}^{(t)}$ such that $\min_{k \in \mathcal{K}}\{R_k(\boldsymbol{\phi}^{(t)})/\mu_k\} \ge \min_{k \in \mathcal{K}}\{R_k(\boldsymbol{\phi}^{(t-1)})/\mu_k\}$, where $\boldsymbol{\phi}^{(t-1)}$ is found at the previous iteration $t-1$. To do so, we first define an auxiliary function as follows:

$$F_k(\boldsymbol{\phi}, R) = (2^{\mu_k R} - 1)(\boldsymbol{\phi}^H \boldsymbol{K}_k \boldsymbol{\phi} + \sigma_d^2) - p_k \boldsymbol{\phi}^H \boldsymbol{S}_k \boldsymbol{\phi}, \forall k \in \mathcal{K}. \tag{15}$$

At iteration t, we update $\boldsymbol{\phi}^{(t)}$ by solving the following problem:

$$\min_{\boldsymbol{\phi}} \max_{k \in \mathcal{K}} F_k(\boldsymbol{\phi}, R^{(t-1)}) \tag{16}$$

$$\text{s.t.} \quad |\phi_{i,m}| \le 1, \forall m \in \{1, .., M_i\}, i \in \mathcal{L}, \tag{17}$$

where

$$R^{(t-1)} = \min_{k \in \mathcal{K}}\{R_k(\boldsymbol{\phi}^{(t-1)})/\mu_k\} \tag{18}$$

is the sum-rate obtained from previous iteration, with $R_k(\boldsymbol{\phi}) = \log_2(1 + \text{SINR}_k)$ is defined in Section II-C. Because the function $F_k(\boldsymbol{\phi}, R^{(t-1)})$ is not convex with respect to $\boldsymbol{\phi}$, hence we apply SCA method to approximate this function by its first-order Taylor expansion at previous local point $\boldsymbol{\phi}^{(t-1)}$, as follows:

$$\begin{aligned} &F_k(\boldsymbol{\phi}, R^{(t-1)}) \le (2^{\mu_k R^{(t-1)}} - 1)(\boldsymbol{\phi}^H \boldsymbol{K}_k \boldsymbol{\phi} + \sigma_d^2) \\ &- p_k \left(2\text{Re}\{(\boldsymbol{\phi}^{(t-1)})^H \boldsymbol{S}_k \boldsymbol{\phi}\} - (\boldsymbol{\phi}^{(t-1)})^H \boldsymbol{S}_k \boldsymbol{\phi}^{(t-1)}\right) \\ &\triangleq \tilde{F}_k(\boldsymbol{\phi}, \boldsymbol{\phi}^{(t-1)}, R^{(t-1)}) \end{aligned} \tag{19}$$

Besides, by introducing an auxiliary variable z, problem (16) can be approximated as the following problem:

$$\min_{\boldsymbol{\phi}, z} \quad z \tag{20a}$$

$$\text{s.t.} \quad \tilde{F}_k(\boldsymbol{\phi}, \boldsymbol{\phi}^{(t-1)}, R^{(t-1)}) \leq z, \quad \forall k \in \mathcal{K}, \tag{20b}$$
$$(17). \tag{20c}$$

It can be seen that the above problem is a convex problem, which can be easily solved by the CVX solver [35]. Notice that $(\boldsymbol{\phi}^{(t-1)}, z = 0)$ is a feasible solution to problem (20). Therefore, we have $z^\star \leq 0$ and $\max_k\{\tilde{F}_k(\tilde{\boldsymbol{\phi}}^\star, \boldsymbol{\phi}^{(t-1)}, R^{(t-1)})\} \leq 0$, which implies that $\max_k\{F_k(\tilde{\boldsymbol{\phi}}^\star, R^{(t-1)})\} \leq 0$, or $\min_{k\in\mathcal{K}}\{R_k(\tilde{\boldsymbol{\phi}}^\star)/\mu_k\} \geq \min_{k\in\mathcal{K}}\{R_k(\boldsymbol{\phi}^{(t-1)})/\mu_k\}$. This means that we always find $\tilde{\boldsymbol{\phi}}^\star$ that leads to non-decreasing sum-rate R at each iteration t. After the SCA-based algorithm converges, the final phase shift solution $\tilde{\boldsymbol{\phi}}^\star$ is projected onto the set $\mathcal{F} = \{\boldsymbol{\phi} : |\phi_{i,m}| = 1, \forall i, m\}$ to recover the original solution $\boldsymbol{\phi}^\star$ that satisfies (13c). The optimal achievable sum-rate $R^\star$ is achieved as

$$R^\star = \min_{k\in\mathcal{K}} \frac{R_k(\boldsymbol{\phi}^\star)}{\mu_k}. \tag{21}$$

The algorithm for solving (14) is summarized in Algorithm 1.

Algorithm 1 SCA-based algorithm for solving (14)

Input: Initialize iteration index $t = 0, \boldsymbol{\phi}^{(0)}, R^{(0)}$, and tolerance $\epsilon > 0$.
Output: $R^\star, \boldsymbol{\phi}^\star$.
1: **Repeat**
2: Given $\boldsymbol{\phi}^{(t-1)}$ and $R^{(t-1)}$, solve problem (20) to obtain $\tilde{\boldsymbol{\phi}}^\star, z^\star$ and update $\boldsymbol{\phi}^{(t)} = \tilde{\boldsymbol{\phi}}^\star$;
3: Given $\boldsymbol{\phi}^{(t-1)}$, update $R^{(t)}$ based on (18);
4: $t \leftarrow t + 1$;
5: **Until** The algorithm convergence is met with given tolerance ϵ.
6: Optimal phase shift vector $\boldsymbol{\phi}^\star$ is achieved by projecting $\tilde{\boldsymbol{\phi}}^\star$ onto the set $\mathcal{F}$.
7: Optimal achievable sum-rate $R^\star$ is achieved by (21).

B. Sum-rate Maximization

In this subsection, we optimize the IRS beamforming to maximize the sum rate at the destinations, subject to the phase shift constraint at all IRSs. This problem is formulated as

$$\max_{\boldsymbol{\phi}} \quad \sum_{k=1}^{K} R_k(\boldsymbol{\phi}) \tag{22a}$$
$$\text{s.t.} \quad |\phi_{i,m}| = 1, \quad \forall m \in \{1, ..., M_i\}, \forall i \in \mathcal{L} \tag{22b}$$

1) Equivalent transformation: The sum-rate maximization is written as

$$\max_{\boldsymbol{\phi}} \quad \sum_{k=1}^{K} \log_2\left(1 + \frac{p_k(\boldsymbol{\phi}^H \boldsymbol{S}_k \boldsymbol{\phi})}{\boldsymbol{\phi}^H \boldsymbol{K}_k \boldsymbol{\phi} + \sigma_d^2}\right) \tag{23a}$$
$$\text{s.t.} \quad (22b) \tag{23b}$$

Throughout the paper, the notation $\log(\cdot)$ stands for the natural logarithm function. By using the change-of-base rule, and then omitting the factor $\log_2(e)$ without affecting the problem, problem (23) is equivalent to

$$\max_{\boldsymbol{\phi}} \quad \sum_{k=1}^{K} \log\left(1 + \frac{p_k(\boldsymbol{\phi}^H \boldsymbol{S}_k \boldsymbol{\phi})}{\boldsymbol{\phi}^H \boldsymbol{K}_k \boldsymbol{\phi} + \sigma_d^2}\right) \tag{24a}$$
$$\text{s.t.} \quad (22b) \tag{24b}$$

To deal with the sum-of-logarithmic-of-ratios problem, we apply the fractional programming approach [36], in which the *Lagrangian dual transform* and *quadratic transform* are employed to take the ratio out of the logarithm and decouple the numerator and denominator of the resulting ratio term, respectively. We proceed according to the following steps:

Step 1: Lagrangian dual transform

Introducing a vector of auxiliary variables $\boldsymbol{\alpha} = [\alpha_1, ..., \alpha_K]^T$, with $\alpha_k \geq 0, \forall k \in \mathcal{K}$, the logarithm function in the objective function is written as

$$\log\left(1 + \frac{p_k(\boldsymbol{\phi}^H \boldsymbol{S}_k \boldsymbol{\phi})}{\boldsymbol{\phi}^H \boldsymbol{K}_k \boldsymbol{\phi} + \sigma_d^2}\right) = \max_{\alpha_k \geq 0}\left\{\log(1 + \alpha_k) - \alpha_k + (1 + \alpha_k)\frac{p_k(\boldsymbol{\phi}^H \boldsymbol{S}_k \boldsymbol{\phi})}{\boldsymbol{\phi}^H (p_k \boldsymbol{S}_k + \boldsymbol{K}_k)\boldsymbol{\phi} + \sigma_d^2}\right\}. \tag{25}$$

Problem (24) is then reformulated as

$$\max_{\boldsymbol{\phi}, \boldsymbol{\alpha}} \quad f_{S1}(\boldsymbol{\phi}, \boldsymbol{\alpha}) \tag{26a}$$
$$\text{s.t.} \quad (22b), \tag{26b}$$
$$\alpha_k \geq 0, \quad \forall k \in \mathcal{K}, \tag{26c}$$

where

$$f_{S1}(\boldsymbol{\phi}, \boldsymbol{\alpha}) \triangleq \sum_{k=1}^{K} \log(1 + \alpha_k) - \sum_{k=1}^{K} \alpha_k + \sum_{k=1}^{K} \frac{p_k(1 + \alpha_k)(\boldsymbol{\phi}^H \boldsymbol{S}_k \boldsymbol{\phi})}{\boldsymbol{\phi}^H (p_k \boldsymbol{S}_k + \boldsymbol{K}_k)\boldsymbol{\phi} + \sigma_d^2}. \tag{27}$$

Step 2: Quadratic transform

For the given $\boldsymbol{\alpha}$, we focus on maximizing the sum-of-ratios term in the objective function (27), as follows:

$$\max_{\boldsymbol{\phi}} \quad \sum_{k=1}^{K} \frac{p_k(1 + \alpha_k)(\boldsymbol{\phi}^H \boldsymbol{S}_k \boldsymbol{\phi})}{\boldsymbol{\phi}^H (p_k \boldsymbol{S}_k + \boldsymbol{K}_k)\boldsymbol{\phi} + \sigma_d^2} \tag{28a}$$
$$\text{s.t.} \quad (22b) \tag{28b}$$

Using the quadratic transform technique [36], the above problem is equivalent to

$$\max_{\boldsymbol{\phi}, \boldsymbol{\beta}} \quad f_{S2}(\boldsymbol{\phi}, \boldsymbol{\beta}) \tag{29a}$$
$$\text{s.t.} \quad (22b), \tag{29b}$$
$$\beta_k \in \mathbb{C}, \quad \forall k \in \mathcal{K}, \tag{29c}$$

where

$$f_{S2}(\boldsymbol{\phi},\boldsymbol{\beta}) \triangleq \sum_{k=1}^{K} 2\sqrt{p_k(1+\alpha_k)}\mathrm{Re}\{\beta_k^*(\boldsymbol{a}_k^H\boldsymbol{\phi})\} - \sum_{k=1}^{K}|\beta_k|^2\big(\boldsymbol{\phi}^H(p_k\boldsymbol{S}_k+\boldsymbol{K}_k)\boldsymbol{\phi}+\sigma_d^2\big), \tag{30}$$

where $\boldsymbol{\beta}=[\beta_1,...,\beta_K]^T$ is a vector of auxiliary variables, with $\beta_k\in\mathbb{C},\forall k\in\mathcal{K}$, and $\boldsymbol{a}_k$ is the vector defined in (8). Thus, according to this step, problem (26) is further transformed into the following problem:

$$\max_{\boldsymbol{\phi},\boldsymbol{\alpha},\boldsymbol{\beta}} \quad f_{S3}(\boldsymbol{\phi},\boldsymbol{\alpha},\boldsymbol{\beta}) \tag{31a}$$

$$\text{s.t.} \quad (22b),(26c),(29c) \tag{31b}$$

where

$$f_{S3}(\boldsymbol{\phi},\boldsymbol{\alpha},\boldsymbol{\beta}) \triangleq \sum_{k=1}^{K}\log(1+\alpha_k)-\sum_{k=1}^{K}\alpha_k + \sum_{k=1}^{K}2\sqrt{p_k(1+\alpha_k)}\mathrm{Re}\{\beta_k^*(\boldsymbol{a}_k^H\boldsymbol{\phi})\} - \sum_{k=1}^{K}|\beta_k|^2\big(\boldsymbol{\phi}^H(p_k\boldsymbol{S}_k+\boldsymbol{K}_k)\boldsymbol{\phi}+\sigma_d^2\big). \tag{32}$$

In the following, we iteratively update $\boldsymbol{\alpha},\boldsymbol{\beta}$, and $\boldsymbol{\phi}$ in an alternating manner. Specifically, at each iteration, the problem is maximized with respect to one variable while the other variables are fixed. Specifically, $\boldsymbol{\alpha}$ and $\boldsymbol{\beta}$ are updated through the following proposition.

Proposition 2. *a) For the fixed $(\boldsymbol{\phi},\boldsymbol{\beta})$, and $k\in\mathcal{K}$, optimal solution $\alpha_k^\star$ is found in the following closed form:*

$$\alpha_k^\star=\frac{\xi_k^2+|\xi_k|\sqrt{\xi_k^2+4}}{2}, \tag{33}$$

where $\xi_k=\sqrt{p_k}Re\{\beta_k^*(\boldsymbol{a}_k^H\boldsymbol{\phi})\}$.
b) For the fixed $(\boldsymbol{\phi},\boldsymbol{\alpha})$, and $k\in\mathcal{K}$, optimal solution $\beta_k^\star$ is found in the following closed form:

$$\beta_k^\star=\frac{\sqrt{p_k(1+\alpha_k)}(\boldsymbol{a}_k^H\boldsymbol{\phi})}{\boldsymbol{\phi}^H(p_k\boldsymbol{S}_k+\boldsymbol{K}_k)\boldsymbol{\phi}+\sigma_d^2}. \tag{34}$$

Proof. For the fixed $(\boldsymbol{\phi},\boldsymbol{\beta})$, $f_{S3}(\boldsymbol{\phi},\boldsymbol{\alpha},\boldsymbol{\beta})$ is a concave function of $\alpha_k,\forall k\in\mathcal{K}$, and the optimal $\alpha_k^\star$ is then obtained by solving the equation $\frac{\partial f_{S3}(\boldsymbol{\phi},\boldsymbol{\alpha},\boldsymbol{\beta})}{\partial\alpha_k}=0$. Similarly, for the fixed $(\boldsymbol{\phi},\boldsymbol{\alpha})$, $f_{S3}(\boldsymbol{\phi},\boldsymbol{\alpha},\boldsymbol{\beta})$ is also a concave function of $\beta_k,\forall k\in\mathcal{K}$. The optimal $\beta^\star$ is then obtained by solving the equation $\frac{\partial f_{S3}(\boldsymbol{\phi},\boldsymbol{\alpha},\boldsymbol{\beta})}{\partial\beta_k}=0$. □

2) Optimizing phase shift of IRS: For the fixed $(\boldsymbol{\alpha},\boldsymbol{\beta})$, problem (31) is reduced as

$$\max_{\boldsymbol{\phi}} \quad f_{S4}(\boldsymbol{\phi}) \tag{35a}$$

$$\text{s.t.} \quad (22b), \tag{35b}$$

where

$$f_{S4}(\boldsymbol{\phi}) \triangleq \sum_{k=1}^{K}2\sqrt{p_k(1+\alpha_k)}\mathrm{Re}\{\beta_k^*(\boldsymbol{a}_k^H\boldsymbol{\phi})\} - \sum_{k=1}^{K}|\beta_k|^2\big(\boldsymbol{\phi}^H(p_k\boldsymbol{S}_k+\boldsymbol{K}_k)\boldsymbol{\phi}\big). \tag{36}$$

For simplicity, let $\boldsymbol{a}\triangleq\sum_{k=1}^{K}2\sqrt{p_k(1+\alpha_k)}\beta_k\boldsymbol{a}_k$ and $\mathbf{A}\triangleq\sum_{k=1}^{K}|\beta_k|^2(p_k\boldsymbol{S}_k+\boldsymbol{K}_k)$, the function $f_{S4}(\boldsymbol{\phi})$ becomes the following:

$$f_{S4}(\boldsymbol{\phi})=\mathrm{Re}\{\boldsymbol{a}^H\boldsymbol{\phi}\}-\boldsymbol{\phi}^H\boldsymbol{A}\boldsymbol{\phi}. \tag{37}$$

To solve problem (35), we employ the ADMM method [37]–[39]. The main idea of this method is to decompose the problem into parallel subproblems that can be solved in closed form. Particularly, we first rewrite this problem so that it can be fit into the ADMM framework

$$\max_{\boldsymbol{\varphi},\boldsymbol{\phi}} \quad f_{S5}(\boldsymbol{\varphi},\boldsymbol{\phi})\triangleq f_{S4}(\boldsymbol{\phi})-\iota_{\mathcal{F}}(\boldsymbol{\varphi}) \tag{38a}$$

$$\text{s.t.} \quad \boldsymbol{\varphi}-\boldsymbol{\phi}=0, \tag{38b}$$

where $\boldsymbol{\varphi}$ is an auxiliary variable for $\boldsymbol{\phi}$, $\iota_{\mathcal{F}}(\cdot)$ is the indicator function of the set (defined in Section III-A) $\mathcal{F}=\{\boldsymbol{\phi}=\{\phi_{i,m}\}:|\phi_{i,m}|=1,m\in\{1,...,M_i\},i\in\{1,...,L\}\}$, in which $\iota_{\mathcal{F}}(z)=0$ if $z\in\mathcal{F}$; otherwise $\iota_{\mathcal{F}}(z)=\infty$. The constraint (38b) is the consensus constraint. Then, the augmented Lagrangian function is given by

$$\mathcal{L}_\rho(\boldsymbol{\varphi},\boldsymbol{\phi},\boldsymbol{\lambda})=f_{S5}(\boldsymbol{\varphi},\boldsymbol{\phi})+\mathrm{Re}\{\boldsymbol{\lambda}^H(\boldsymbol{\varphi}-\boldsymbol{\phi})\}-\frac{\rho}{2}\|\boldsymbol{\varphi}-\boldsymbol{\phi}\|_2^2, \tag{39}$$

where $\boldsymbol{\lambda}\in\mathbb{C}^{\sum_{i=1}^{L}M_i\times 1}$ is the Lagrange multiplier vector associated with the constraint $\boldsymbol{\varphi}-\boldsymbol{\phi}=0$, and $\rho>0$ is a penalty parameter for $\boldsymbol{\varphi}-\boldsymbol{\phi}\neq 0$. The dual function is then given by

$$\mathcal{G}_\rho(\boldsymbol{\lambda})=\max_{\boldsymbol{\varphi},\boldsymbol{\phi}}\mathcal{L}_\rho(\boldsymbol{\varphi},\boldsymbol{\phi},\boldsymbol{\lambda}).$$

Thus, the dual problem is formulated as

$$\min_{\boldsymbol{\lambda}} \quad \mathcal{G}_\rho(\boldsymbol{\lambda}). \tag{40}$$

To solve the primal problem (38), we apply the ADMM which consists of the following iterations:

$$\boldsymbol{\varphi}^{t+1}=\arg\max_{\boldsymbol{\varphi}\in\boldsymbol{\mathcal{F}}}\mathcal{L}_\rho(\boldsymbol{\varphi},\boldsymbol{\phi}^t,\boldsymbol{\lambda}^t), \tag{41}$$

$$\boldsymbol{\phi}^{t+1}=\arg\max_{\boldsymbol{\phi}}\mathcal{L}_\rho(\boldsymbol{\varphi}^{t+1},\boldsymbol{\phi},\boldsymbol{\lambda}^t), \tag{42}$$

$$\boldsymbol{\lambda}^{t+1}=\boldsymbol{\lambda}^t-\rho(\boldsymbol{\varphi}^{t+1}-\boldsymbol{\phi}^{t+1}). \tag{43}$$

Solving the maximization problem with respect to $\boldsymbol{\varphi}$ in (41) given $(\boldsymbol{\phi}^t,\boldsymbol{\lambda}^t)$ implies that

$$\boldsymbol{\varphi}^{t+1}=\mathcal{P}_{\mathcal{F}}(\boldsymbol{\phi}^t+\frac{1}{\rho}\boldsymbol{\lambda}^t), \tag{44}$$

where $\mathcal{P}_{\mathcal{F}}$ is the projection onto set $\mathcal{F}$. Therefore, the image of $\boldsymbol{\varphi}^{t+1}$ through this projection is specified in closed form as

follows:

$$\varphi_{i,m}^{t+1} = \begin{cases} \frac{\phi_{i,m}^t + \frac{1}{\rho}\lambda_{i,m}^t}{|\phi_{i,m}^t + \frac{1}{\rho}\lambda_{i,m}^t|} & \text{if } \phi_{i,m}^t + \frac{1}{\rho}\lambda_{i,m}^t \neq 0, \\ \varphi_{i,m}^t & \text{otherwise,} \end{cases} \tag{45}$$

where $\phi_{i,m}^t, \varphi_{i,m}^t$, and $\lambda_{i,m}^t$ are the (i,m)-th components of $\boldsymbol{\phi}^t, \boldsymbol{\varphi}^t$, and $\boldsymbol{\lambda}^t$, respectively. It can be seen that the maximization problem in (42) given $(\boldsymbol{\varphi}^{t+1}, \boldsymbol{\lambda}^t)$ is concave; hence, the solution $\boldsymbol{\phi}^{t+1}$ can be obtained by setting the first derivative with respect to $\boldsymbol{\phi}$ to zero. This implies that

$$\rho(\boldsymbol{\phi}^{t+1} - \boldsymbol{\varphi}^{t+1}) = \boldsymbol{a} - 2\boldsymbol{A}\boldsymbol{\phi}^{t+1} - \boldsymbol{\lambda}^t. \tag{46}$$

This is equivalent to

$$\boldsymbol{\phi}^{t+1} = \left(2\boldsymbol{A} + \rho \boldsymbol{I}_{\sum_{i=1}^{L} M_i}\right)^{-1} \left(\boldsymbol{a} - \boldsymbol{\lambda}^t + \rho\boldsymbol{\varphi}^{t+1}\right). \tag{47}$$

The algorithms for solving problems (35) and (31) are presented in Algorithm 2 and Algorithm 3, respectively.

Algorithm 2 ADMM algorithm for solving problem (35)

Input: Initialize a feasible primal-dual point $(\boldsymbol{\varphi}^0, \boldsymbol{\phi}^0, \boldsymbol{\lambda}^0)$, choose the penalty parameter $\rho > 2\sqrt{2}\lambda_{\max}(\mathbf{A})$, and set the iteration index $t = 0$.

Output: Locally optimal phase shift vector $\tilde{\boldsymbol{\phi}}^\star$.

1: **Repeat**
2: Compute φ_i^{t+1} based on (45) in parallel, $\forall i \in \mathcal{L}$;
3: Compute $\boldsymbol{\phi}^{t+1}$ based on (47);
4: Compute λ_i^{t+1} based on (43) in parallel, $\forall i \in \mathcal{L}$;
5: $t \leftarrow t + 1$;
6: **Until** Convergence is reached.

Algorithm 3 Alternating optimization (AO) algorithm for solving problem (31)

Input: Initialize a feasible point $(\boldsymbol{\alpha}^0, \boldsymbol{\beta}^0, \boldsymbol{\phi}^0)$, and set the iteration index $s = 0$.

Output: Locally optimal phase shift vector $\boldsymbol{\phi}^\star$.

1: **Repeat**
2: Compute α_k^{s+1} based on (33) in parallel, $\forall k \in \mathcal{K}$;
3: Compute β_k^{s+1} based on (34) in parallel, $\forall k \in \mathcal{K}$;
4: Apply Algorithm 2 with $\boldsymbol{\phi}^0 = \boldsymbol{\phi}^s$ to obtain the solution $\tilde{\boldsymbol{\phi}}^\star$.
5: Set $\boldsymbol{\phi}^{s+1} = \tilde{\boldsymbol{\phi}}^\star$;
6: $s \leftarrow s + 1$;
7: **Until** Convergence is reached.

Next, we discuss the convergence of Algorithm 2 through the following propositions.

Proposition 3. *Supposing that $\rho > 2\sqrt{2}\lambda_{max}(\boldsymbol{A})$, where $\lambda_{max}(\boldsymbol{A})$ is the maximum eigenvalue of $\boldsymbol{A}$, the sequence $\{\mathcal{L}_\rho(\boldsymbol{\varphi}^t, \boldsymbol{\phi}^t, \boldsymbol{\lambda}^t)\}$ is convergent.*

Proof. This proof is inspired by [40] with certain modifications. To prove the convergence, we need to prove that: $\mathcal{L}_\rho(\boldsymbol{\varphi}^t, \boldsymbol{\phi}^t, \boldsymbol{\lambda}^t)$ is monotonically increasing and bounded above.

- $\mathcal{L}_\rho(\boldsymbol{\varphi}^t, \boldsymbol{\phi}^t, \boldsymbol{\lambda}^t)$ *is monotonically increasing:*
From the update in (41), we obtain the following:

$$\mathcal{L}_\rho(\boldsymbol{\varphi}^t, \boldsymbol{\phi}^t, \boldsymbol{\lambda}^t) - \mathcal{L}_\rho(\boldsymbol{\varphi}^{t+1}, \boldsymbol{\phi}^t, \boldsymbol{\lambda}^t) \leq 0. \tag{48}$$

Furthermore, we can check the strong concavity of function $\mathcal{L}_\rho(\boldsymbol{\varphi}^{t+1}, \boldsymbol{\phi}, \boldsymbol{\lambda}^t)$ (please see Appendix B). Thus, from [41], we have

$$\begin{aligned} \mathcal{L}_\rho(\boldsymbol{\varphi}^{t+1}, \boldsymbol{\phi}^t, \boldsymbol{\lambda}^t) - \mathcal{L}_\rho(\boldsymbol{\varphi}^{t+1}, \boldsymbol{\phi}^{t+1}, \boldsymbol{\lambda}^t) \leq \\ - \frac{\rho}{2}\|\boldsymbol{\phi}^{t+1} - \boldsymbol{\phi}^t\|_2^2. \end{aligned} \tag{49}$$

In addition, from (39) and (43), we have

$$\begin{aligned} &\mathcal{L}_\rho(\boldsymbol{\varphi}^{t+1}, \boldsymbol{\phi}^{t+1}, \boldsymbol{\lambda}^t) - \mathcal{L}_\rho(\boldsymbol{\varphi}^{t+1}, \boldsymbol{\phi}^{t+1}, \boldsymbol{\lambda}^{t+1}) \\ &= \text{Re}\{(\boldsymbol{\lambda}^t)^H(\boldsymbol{\varphi}^{t+1} - \boldsymbol{\phi}^{t+1})\} \\ &\quad - \text{Re}\{(\boldsymbol{\lambda}^{t+1})^H(\boldsymbol{\varphi}^{t+1} - \boldsymbol{\phi}^{t+1})\} \\ &= \text{Re}\{(\boldsymbol{\lambda}^t - \boldsymbol{\lambda}^{t+1})^H(\boldsymbol{\varphi}^{t+1} - \boldsymbol{\phi}^{t+1})\} \\ &= \frac{1}{\rho}\|\boldsymbol{\lambda}^t - \boldsymbol{\lambda}^{t+1}\|_2^2. \end{aligned} \tag{50}$$

Moreover, from (43) and (46), we obtain

$$\boldsymbol{\lambda}^{t+1} = \boldsymbol{a} - 2\boldsymbol{A}\boldsymbol{\phi}^{t+1}, \tag{51}$$

or

$$\boldsymbol{\lambda}^t = \boldsymbol{a} - 2\boldsymbol{A}\boldsymbol{\phi}^t. \tag{52}$$

Combining (48) to (50), we have

$$\begin{aligned} &\mathcal{L}_\rho(\boldsymbol{\varphi}^t, \boldsymbol{\phi}^t, \boldsymbol{\lambda}^t) - \mathcal{L}_\rho(\boldsymbol{\varphi}^{t+1}, \boldsymbol{\phi}^{t+1}, \boldsymbol{\lambda}^{t+1}) \\ &= \mathcal{L}_\rho(\boldsymbol{\varphi}^t, \boldsymbol{\phi}^t, \boldsymbol{\lambda}^t) - \mathcal{L}_\rho(\boldsymbol{\varphi}^{t+1}, \boldsymbol{\phi}^t, \boldsymbol{\lambda}^t) + \mathcal{L}_\rho(\boldsymbol{\varphi}^{t+1}, \boldsymbol{\phi}^t, \boldsymbol{\lambda}^t) \\ &\quad - \mathcal{L}_\rho(\boldsymbol{\varphi}^{t+1}, \boldsymbol{\phi}^{t+1}, \boldsymbol{\lambda}^t) + \mathcal{L}_\rho(\boldsymbol{\varphi}^{t+1}, \boldsymbol{\phi}^{t+1}, \boldsymbol{\lambda}^t) \\ &\quad - \mathcal{L}_\rho(\boldsymbol{\varphi}^{t+1}, \boldsymbol{\phi}^{t+1}, \boldsymbol{\lambda}^{t+1}) \\ &\leq -\frac{\rho}{2}\|\boldsymbol{\phi}^{t+1} - \boldsymbol{\phi}^t\|_2^2 + \frac{1}{\rho}\|\boldsymbol{\lambda}^t - \boldsymbol{\lambda}^{t+1}\|_2^2 \\ &= -\frac{\rho}{2}\|\boldsymbol{\phi}^{t+1} - \boldsymbol{\phi}^t\|_2^2 + \frac{4}{\rho}\|\boldsymbol{A}(\boldsymbol{\phi}^t - \boldsymbol{\phi}^{t+1})\|_2^2 \\ &\leq -\frac{\rho}{2}\|\boldsymbol{\phi}^{t+1} - \boldsymbol{\phi}^t\|_2^2 + \frac{4}{\rho}\|\boldsymbol{A}\|^2\|\boldsymbol{\phi}^t - \boldsymbol{\phi}^{t+1}\|_2^2 \\ &\leq -\frac{\rho}{2}\|\boldsymbol{\phi}^{t+1} - \boldsymbol{\phi}^t\|_2^2 + \frac{4}{\rho}\lambda_{\max}^2(\boldsymbol{A})\|\boldsymbol{\phi}^t - \boldsymbol{\phi}^{t+1}\|_2^2 \\ &= \eta\|\boldsymbol{\phi}^t - \boldsymbol{\phi}^{t+1}\|_2^2, \end{aligned} \tag{53}$$

where $\eta \triangleq \frac{4}{\rho}\lambda_{\max}^2(\boldsymbol{A}) - \frac{\rho}{2}$ and the second equality is obtained by using (51) and (52). According to the choice of ρ, i.e., $\rho > 2\sqrt{2}\lambda_{\max}(\mathbf{A})$, and thus $\eta < 0$. As a result, we obtain $\mathcal{L}_\rho(\boldsymbol{\varphi}^t, \boldsymbol{\phi}^t, \boldsymbol{\lambda}^t) \leq \mathcal{L}_\rho(\boldsymbol{\varphi}^{t+1}, \boldsymbol{\phi}^{t+1}, \boldsymbol{\lambda}^{t+1})$.

- $\mathcal{L}_\rho(\boldsymbol{\varphi}^t, \boldsymbol{\phi}^t, \boldsymbol{\lambda}^t)$ *is upper bounded:*
We have

$$\begin{aligned} &\mathcal{L}_\rho(\boldsymbol{\varphi}^t, \boldsymbol{\phi}^t, \boldsymbol{\lambda}^t) = \text{Re}\{\boldsymbol{a}^H\boldsymbol{\phi}^t\} - (\boldsymbol{\phi}^t)^H\boldsymbol{A}\boldsymbol{\phi}^t \\ &+ \text{Re}\{(\boldsymbol{\lambda}^t)^H(\boldsymbol{\varphi}^t - \boldsymbol{\phi}^t)\} - \frac{\rho}{2}\|\boldsymbol{\varphi}^t - \boldsymbol{\phi}^t\|_2^2, \text{ for } \boldsymbol{\varphi}^t \in \mathcal{F}. \end{aligned} \tag{54}$$

Substituting the expression in (52) into (54) yields

$$\mathcal{L}_\rho(\boldsymbol{\varphi}^t, \boldsymbol{\phi}^t, \boldsymbol{\lambda}^t) = \text{Re}\{\boldsymbol{a}^H\boldsymbol{\phi}^t\} - (\boldsymbol{\phi}^t)^H\boldsymbol{A}\boldsymbol{\phi}^t$$

$$
\begin{aligned}
&+ \mathrm{Re}\{(\boldsymbol{a}-2\boldsymbol{A}\boldsymbol{\phi}^t)^H(\boldsymbol{\varphi}^t-\boldsymbol{\phi}^t)\} - \frac{\rho}{2}\|\boldsymbol{\varphi}^t-\boldsymbol{\phi}^t\|_2^2 \\
&= \mathrm{Re}\{\boldsymbol{a}^H\boldsymbol{\varphi}^t\} - \left((\boldsymbol{\phi}^t)^H(\boldsymbol{A}-\frac{2}{\rho}\boldsymbol{A}\boldsymbol{A})\boldsymbol{\phi}^t\right) \\
&\quad - \frac{\rho}{2}\|\frac{2}{\rho}\boldsymbol{A}\boldsymbol{\phi}^t+(\boldsymbol{\varphi}^t-\boldsymbol{\phi}^t)\|_2^2 \\
&\le \mathrm{Re}\{\boldsymbol{a}^H\boldsymbol{\varphi}^t\}, \qquad (55)
\end{aligned}
$$

where the last inequality holds because $\boldsymbol{A}-\frac{2}{\rho}\boldsymbol{A}\boldsymbol{A}\succeq 0$ for $\rho > 2\lambda_{\max}(\boldsymbol{A})$. In addition, applying the Cauchy–Schwarz inequality implies that $|\mathrm{Re}\{\boldsymbol{a}^H\boldsymbol{\varphi}^t\}| \le \|\boldsymbol{\varphi}^t\|_2\|\boldsymbol{a}\|_2 = \sqrt{\sum_{i=1}^L M_i}\|\boldsymbol{a}\|_2 < \infty$, for $\boldsymbol{\varphi}^t \in \mathcal{F}$. Hence, $\mathcal{L}_\rho(\boldsymbol{\varphi}^t,\boldsymbol{\phi}^t,\boldsymbol{\lambda}^t)$ is bounded from above.

Therefore, the sequence $\{\mathcal{L}_\rho(\boldsymbol{\varphi}^t,\boldsymbol{\phi}^t,\boldsymbol{\lambda}^t)\}$ is guaranteed to converge. This completes the proof. □

The following proposition states that every limit point generated by the ADMM in Algorithm 2 is a Karush-Kuhn-Tucker (KKT) point of problem (35).

Proposition 4. *Every limit point generated by the ADMM method in Algorithm 2 is a Karush-Kuhn-Tucker (KKT) point of problem (35).*

Proof. This proof is inspired by [40] with certain modifications. From (53), we have

$$\mathcal{L}_\rho(\boldsymbol{\varphi}^{t+1},\boldsymbol{\phi}^{t+1},\boldsymbol{\lambda}^{t+1}) - \mathcal{L}_\rho(\boldsymbol{\varphi}^t,\boldsymbol{\varphi}^t,\boldsymbol{\lambda}^t) \ge -\eta\|\boldsymbol{\phi}^{t+1}-\boldsymbol{\phi}^t\|_2^2. \qquad (56)$$

By summing over t from 0 to $T-1$, we obtain

$$\mathcal{L}_\rho(\boldsymbol{\varphi}^T,\boldsymbol{\phi}^T,\boldsymbol{\lambda}^T) - \mathcal{L}_\rho(\boldsymbol{\varphi}^0,\boldsymbol{\phi}^0,\boldsymbol{\lambda}^0) \ge -\eta\sum_{t=0}^{T-1}\|\boldsymbol{\phi}^{t+1}-\boldsymbol{\phi}^t\|_2^2. \qquad (57)$$

Letting $T\to\infty$ and using the fact that $\{\mathcal{L}_\rho(\boldsymbol{\varphi}^t,\boldsymbol{\phi}^t,\boldsymbol{\lambda}^t)\}$ is convergent (by Proposition 3), it is implied that the series $\sum_{t=0}^{\infty}\|\boldsymbol{\phi}^{t+1}-\boldsymbol{\phi}^t\|_2^2$ is convergent. Thus,

$$\lim_{t\to\infty}\|\boldsymbol{\phi}^{t+1}-\boldsymbol{\phi}^t\|_2 = 0. \qquad (58)$$

In addition, from (51), (52), and (43), we have

$$\lim_{t\to\infty}\|\boldsymbol{\lambda}^{t+1}-\boldsymbol{\lambda}^t\|_2 = 0, \lim_{t\to\infty}\|\boldsymbol{\phi}^{t+1}-\boldsymbol{\varphi}^{t+1}\|_2 = 0. \qquad (59)$$

Let $\boldsymbol{\phi}^\dagger$ denote the limit point of the sequence $\{\boldsymbol{\phi}^t\}$. Then, there exists a subsequence $\{\boldsymbol{\phi}^{t_j}\}$ of the sequence $\{\boldsymbol{\phi}^t\}$ that converges to $\boldsymbol{\phi}^\dagger$. It follows from (58) and (59) that

$$\lim_{t_j\to\infty}\boldsymbol{\phi}^{t_j+1} = \lim_{t_j\to\infty}\boldsymbol{\phi}^{t_j} = \boldsymbol{\phi}^\dagger, \qquad (60)$$

$$\lim_{t_j\to\infty}\boldsymbol{\lambda}^{t_j+1} = \lim_{t_j\to\infty}\boldsymbol{\lambda}^{t_j} = \lim_{t_j\to\infty}(\boldsymbol{a}-2\boldsymbol{A}\boldsymbol{\phi}^{t_j}) = \boldsymbol{a}-2\boldsymbol{A}\boldsymbol{\phi}^\dagger, \qquad (61)$$

$$\lim_{t_j\to\infty}\boldsymbol{\varphi}^{t_j+1} = \lim_{t_j\to\infty}\boldsymbol{\phi}^{t_j+1} = \boldsymbol{\phi}^\dagger. \qquad (62)$$

From (62), we obtain

$$\boldsymbol{\phi}^\dagger \in \mathcal{F}. \qquad (63)$$

In addition, from (41) we have $\mathcal{L}_\rho(\boldsymbol{\varphi}^{t+1},\boldsymbol{\phi}^t,\boldsymbol{\lambda}^t) \ge \mathcal{L}_\rho(\boldsymbol{\varphi},\boldsymbol{\phi}^t,\boldsymbol{\lambda}^t), \forall\boldsymbol{\varphi}\in\mathcal{F}$. Thus

$$\lim_{t_j\to\infty}\mathcal{L}_\rho(\boldsymbol{\varphi}^{t_j+1},\boldsymbol{\phi}^{t_j},\boldsymbol{\lambda}^{t_j}) \ge \lim_{t_j\to\infty}\mathcal{L}_\rho(\boldsymbol{\varphi},\boldsymbol{\phi}^{t_j},\boldsymbol{\lambda}^{t_j}), \forall\boldsymbol{\varphi}\in\mathcal{F}. \qquad (64)$$

This is equivalent to

$$\mathcal{L}_\rho(\boldsymbol{\phi}^\dagger,\boldsymbol{\phi}^\dagger,\boldsymbol{a}-2\boldsymbol{A}\boldsymbol{\phi}^\dagger) \ge \mathcal{L}_\rho(\boldsymbol{\varphi},\boldsymbol{\phi}^\dagger,\boldsymbol{a}-2\boldsymbol{A}\boldsymbol{\phi}^\dagger), \forall\boldsymbol{\varphi}\in\mathcal{F}. \qquad (65)$$

This means that $\boldsymbol{\phi}^\dagger = \arg\max_{\boldsymbol{\varphi}\in\mathcal{F}}\mathcal{L}_\rho(\boldsymbol{\varphi},\boldsymbol{\phi}^\dagger,\boldsymbol{a}-2\boldsymbol{A}\boldsymbol{\phi}^\dagger)$. Thus, it satisfies the first-order optimality condition

$$\boldsymbol{a}-2\boldsymbol{A}\boldsymbol{\phi}^\dagger+\boldsymbol{\nu}^T\boldsymbol{\phi}^\dagger = 0, \qquad (66)$$

where $\boldsymbol{\nu}$ is the dual variable vector associated with unit-modulus constraint of problem (35). It can be verified that (63) and (66) constitute the KKT conditions for problem (35). This completes the proof. □

Remark. *From Proposition 4, it is worth mentioning that although Algorithm 2 is convergent, its solution need not to be a global solution owing to the non-convexity of problem (35).*

The following proposition guarantees the convergence of Algorithm 3.

Proposition 5. *By applying Algorithm 3, the value of the objective function in problem (31) is nondecreasing if the solution $\boldsymbol{\phi}^{s+1}$ in the $(s+1)$-th iteration satisfies the following constraint*

$$f_{S3}(\boldsymbol{\phi}^s,\boldsymbol{\alpha}^s,\boldsymbol{\beta}^s) \le f_{S3}(\boldsymbol{\phi}^{s+1},\boldsymbol{\alpha}^s,\boldsymbol{\beta}^s), \qquad (67)$$

for the given $(\boldsymbol{\alpha}^s,\boldsymbol{\beta}^s)$.

Proof. We can verify that the objective value of $f_{S3}(\boldsymbol{\phi},\boldsymbol{\alpha},\boldsymbol{\beta})$ is non-decreasing after each iteration. Indeed, we have

$$
\begin{aligned}
f_{S3}(\boldsymbol{\phi}^s,\boldsymbol{\alpha}^s,\boldsymbol{\beta}^s) &\overset{(a)}{\le} f_{S3}(\boldsymbol{\phi}^{s+1},\boldsymbol{\alpha}^s,\boldsymbol{\beta}^s) \\
&\overset{(b)}{\le} f_{S3}(\boldsymbol{\phi}^{s+1},\boldsymbol{\alpha}^{s+1},\boldsymbol{\beta}^{s+1}),
\end{aligned} \qquad (68)
$$

where (a) holds owing to condition (67) for the given $(\boldsymbol{\alpha}^s,\boldsymbol{\beta}^s)$, and (b) holds because $(\boldsymbol{\alpha}^{s+1},\boldsymbol{\beta}^{s+1})$ is the optimal solution to problem (31) for the given $\boldsymbol{\phi}^{s+1}$. □

C. Complexity Analysis

In Algorithm 1, in each iteration, the complexity for computing $\boldsymbol{\phi}^H\boldsymbol{S}_k\boldsymbol{\phi}$ and $\boldsymbol{\phi}^H\boldsymbol{K}_k\boldsymbol{\phi}$ for $k\in\mathcal{K}$ is $\mathcal{O}(M^2)$, where $M=\sum_{i=1}^L M_i$. In step 2, we solve problem (20) by using the interior-point method (in CVX solver) with the complexity of $\mathcal{O}(M^{3.5})$ [26]. Therefore, the total complexity is $\mathcal{O}(I(M^{3.5}+KM^2))$, where I is the number of iterations required for convergence of Algorithm 1. For Algorithm 3, in each iteration, the complexity for computing α_k (step 2) and β_k (step 3) for $k\in\mathcal{K}$ are $\mathcal{O}(M)$ and $\mathcal{O}(M^2)$, respectively. In step 4, we adopt Algorithm 2 to solve the phase shift vector $\boldsymbol{\phi}$. In each iteration of Algorithm 2, the complexity for updating $\boldsymbol{\varphi}$ is $\mathcal{O}(M)$, for updating $\boldsymbol{\lambda}$ is $\mathcal{O}(M)$, and for updating $\boldsymbol{\phi}$ is $\mathcal{O}(M^3+M^2)$ [42]. Here, the complexity of $\mathcal{O}(M^3)$ is due to the computing the inversion for updating $\boldsymbol{\phi}$ in (47),

which is computed at once and stored in subsequent ADMM iterations. In addition, the computing of maximum eigenvalue of $\boldsymbol{A}$ results in the complexity of $\mathcal{O}(M^3)$. Therefore, the total complexity Algorithm 3 is $\mathcal{O}(I_2(KM^2+I_1M^2+M^3))$, where I_1, I_2 are the number of iterations required for convergence of ADMM and AO algorithm, respectively. More importantly, Algorithm 3 can be accelerated by parallel updating $\{\alpha_k, \beta_k\}$ and $\{\varphi_{i,m}, \lambda_{i,m}\}$ at the sources and the IRS controllers, respectively. On the other hand, SDR-based schemes can be applied to Algorithm 1 and Algorithm 2, which will be used as comparing schemes in the simulation part. In the first comparing scheme for Algorithm 1, [15] solves the problem (14) by a series of feasibility problems together with a bisection search over the sum-rate R. Here, each feasibility problem is solved by applying the SDR technique. It's complexity is $\mathcal{O}\left((M^6+KM^2)\log_2\left(\frac{R_{\text{up}}-R_{\text{low}}}{\epsilon}\right)\right)$, where R_{up} and R_{low} are respectively the upper and lower values of R initialized for the bisection search, ϵ is the predefined accuracy for bisection search. In the second comparing scheme for Algorithm 2, in place of ADMM method, the conventional SDR technique can be applied to find the phase shift solution. This can be done by reformulating problem (35) as an SDP problem by relaxing the rank-one constraint, followed by the Gaussian randomization to reconstruct the rank-one solution. However, the complexity is $\mathcal{O}(M^6)$ [43] resulting in the total complexity of Algorithm 3 being $\mathcal{O}(I_2(KM^2+M^6))$. In general, the complexity of SDR-based algorithms is very high when the number of IRS elements M increases. Moreover, the Gaussian randomization cannot guarantee to generate a rank-one solution. Therefore, we can say that the proposed algorithms have lower complexity than the other conventional approaches, and have polynomial complexity.

IV. Evaluations

A. Simulation Parameters and Comparing Schemes

In this section, the proposed scheme is evaluated in terms of the achievable rate region, achievable sum-rate, and energy efficiency. All channel coefficients are generated from channel model as described in Section II-A. Resulting achievable rates were averaged over 100 independent and random channel realizations. According to [44], [45], the simulation parameters are summarized in Table I. In this evaluation, the comparing schemes can be summarized as follows:

- *SDR-based IRS [15], [46]:* For the achievable rate region characterization, as in [15], we solved problem (14) by solving a feasibility problem together with a bisection search over the sum-rate R. Here, the feasibility problem is solved by applying the SDR technique, which is reformulating the problem as an SDP problem by relaxing the rank-one constraint, followed by the Gaussian randomization to reconstruct the rank-one solution. For the sum-rate maximization, as in [46], the SDR technique was also applied to solve problem (35).
- *Random-phase-shift-based IRS:* The phase shifts are randomly generated within $[0, 2\pi)$.
- *DRL-based IRS [47]:* We transformed the sum-rate maximization problem (23) into a deep reinforcement learning optimization problem by explicitly constructing the state space, action space, and reward. Particularly, the state is determined by the channel information, i.e., $\{\boldsymbol{e}_{i,k}\}, \{\boldsymbol{f}_{k,i}\}$, the action is determined by the phase shift vector $\boldsymbol{\phi}$, and the reward is determined as the achieved sum-rate. Next, we applied the deep deterministic policy gradient (DDPG) algorithm [47] to obtain the phase shifts by gradually maximizing the sum-rate via observing the reward and adjusting the DRL algorithm's parameters.
- *Optimal AF-Relaying [48]:* It considers a half-duplex AF relay. Here, second-order cone programming (SOCP) and SDP problem are formulated, and bisection method is employed. Without decoding the received signals, AF relays require no knowledge of the codebooks used by the transmitters and likely have a lower baseband complexity and fast signal processing.
- *Interference Neutralization (IN) [48]:* It is an near-optimal half-duplex AF relaying scheme that allows the interference to be canceled over the air in the last hop.
- *DF-relaying (selective):* The best one among the half-duplex DF relays is selected based on the achievable rate. Here, the achievable rate is computed by applying maximum ratio combining (MRC) and maximum ratio transmission (MRT) scheme for the data reception and transmission at each DF relay, respectively.
- *DF-relaying (cooperative):* All half-duplex DF relays fully cooperate, i.e. data, channel information, and antenna sharing. This means that all DF relays are treated as one big DF relay. Likewise above, MRC and MRT schemes are applied.

B. Achievable Rate Region

In this subsection, we evaluated the proposed SCA-based approach described in Algorithm 1 for characterizing the achievable region of the IRS-based system, as well as the benchmark schemes described in Subsection IV-A. Particularly, we considered an IRS-relaying network in Fig. 2(a), in which $K = 2$ source-destination pairs are randomly and uniformly distributed in a circle centered at $(0, 0)$ with radius of 10 meters and another one centered at $(100, 0)$ with the same radius, respectively. Two IRSs are placed at $(50, 30)$ and $(60, 30)$, respectively to assist the communication between two pairs. We assume that the transmit powers at all sources are the same, i.e., $p_k = 10$ dBm, for $k \in \{1, 2\}$; the noise variance at the AF/DF relays and destinations are $\sigma_r^2 = \sigma_d^2 = \sigma^2$. For the sake of comparison with AF/DF relay networks, two AF/DF relays with two antennas each are used to assist the communication. Here, the transmit power at each AF/DF relay is set to be the same as the source transmit power, i.e., $p_{\text{AF},i} = p_{\text{DF},i} = 10$ dBm, for $i \in \{1, 2\}$. In addition, to ensure the fair comparison among the IRS-based and conventional relaying systems (AF/DF), we used the same power budget, denoted as P_{budget}, which is set to be 22 dBm. In the following evaluation, IRS-(m, n) denotes m IRSs, each of which is equipped with n IRS elements, and relay-(m, n) denotes m AF/DF relays, each of which is equipped with n active antennas. In Fig. 2(b), when the IRSs

TABLE I
TABLE OF SIMULATION PARAMETERS

Parameters	Values
Bandwidth B	1 MHz
Noise power σ^2	-94 dBm
Path loss model at distance d	$\eta(d) = 30 + 22\log_{10}(d)$ dB
Rician factors κ_1, κ_2	10
Power amplifier efficiency of source, AF, and DF relay $\nu, \nu_{\text{AF}}, \nu_{\text{DF}}$	0.8
Signal processing power of each DF relay $P_{\text{DF},i}^{\text{proc}}$	10 dBm
Circuit power of k-th source and destination $P_{S,k}, P_{D,k}$	10 dBm
Circuit power of each AF and DF relay antenna $P_{\text{AF}}^{\text{ant}}, P_{\text{DF}}^{\text{ant}}$	10 dBm
Circuit power of each IRS element P_I	10 dBm

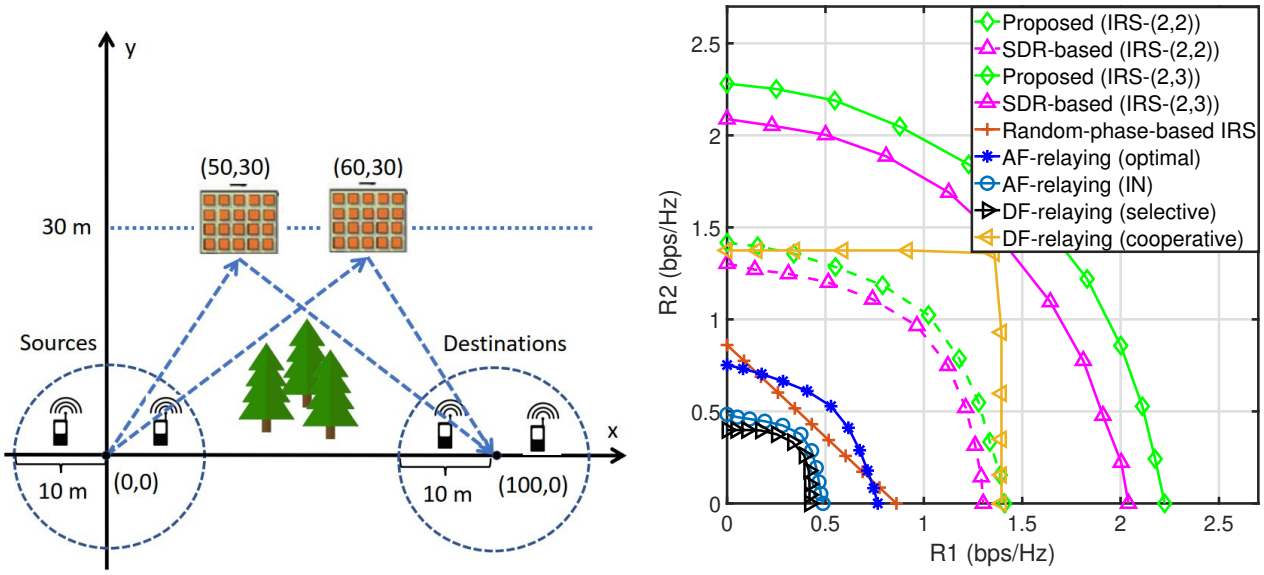

(a) IRS-relaying network.

(b) Achievable region.

Fig. 2. (a) IRS-relaying network, (b) Achievable rate region with IRS-(2,2), IRS-(2,3), and relay-(2,2).

are equipped with $M_1 = M_2 = 2$ reflecting elements each, it can be observed that the achievable rate region of the proposed scheme is larger than other benchmarks except the DF-relaying (cooperative) scheme. However, when increasing the number of IRS elements M_1 and M_2 to above 3, the achievable rate region of the proposed IRS-based transmission becomes larger than the DF-relaying (cooperative) scheme. In comparison with SDR-based IRS scheme, it can be seen that the proposed scheme achieves higher achievable rate over different numbers of IRS elements, e.g., $M_i \in \{2, 3\}$. We should notice that larger number of IRS elements always leads to higher energy consumption. In our simulation, the increasing number of IRS elements only results in 10 dBm higher in power consumption. In this case, the total consumption power is 20.9 dBm, which is still guaranteed to be lower than the provided total power budget with $P_{\text{budget}} = 22$ dBm.

C. Achievable Sum-Rate

In this subsection, we demonstrated the effectiveness of the proposed Algorithm 3 for the achievable sum rate maximization, as compared with the benchmark schemes described in Subsection IV-A. We consider K sources-destination pairs, which are randomly and uniformly distributed in the same circle areas as in the simulation of the achievable rate region. In addition, there are $L = 4$ IRSs, which are placed at $(40, 30)$, $(50, 30)$, $(60, 30)$, and $(70, 30)$, respectively. We assume that the transmit powers at all sources are the same. The noise variance at the AF/DF relays and destinations are assumed as $\sigma_r^2 = \sigma_d^2 = \sigma^2$. For the setup of AF/DF relay systems, four AF/DF relays with six antennas each are used to assist the communication, and the transmit power at each relay is set to be the same as the source transmit power. For fair comparison, the power budget for each system is set to be 42 dBm.

In this simulation, we set the number of source-destination

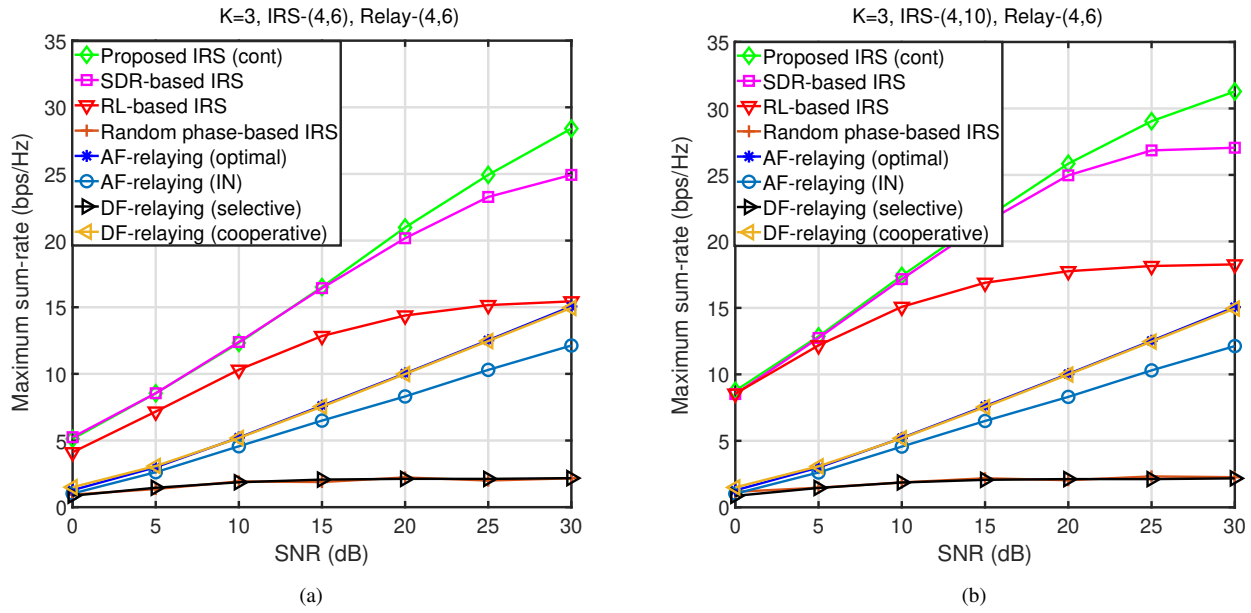

Fig. 3. Maximum sum-rate with $K = 3$ under two settings of IRS and AF/DF relay: **(a)** IRS-(4, 6) and AF/DF relay-(4, 6); **(b)** IRS-(4, 10) and AF/DF relay-(4, 6).

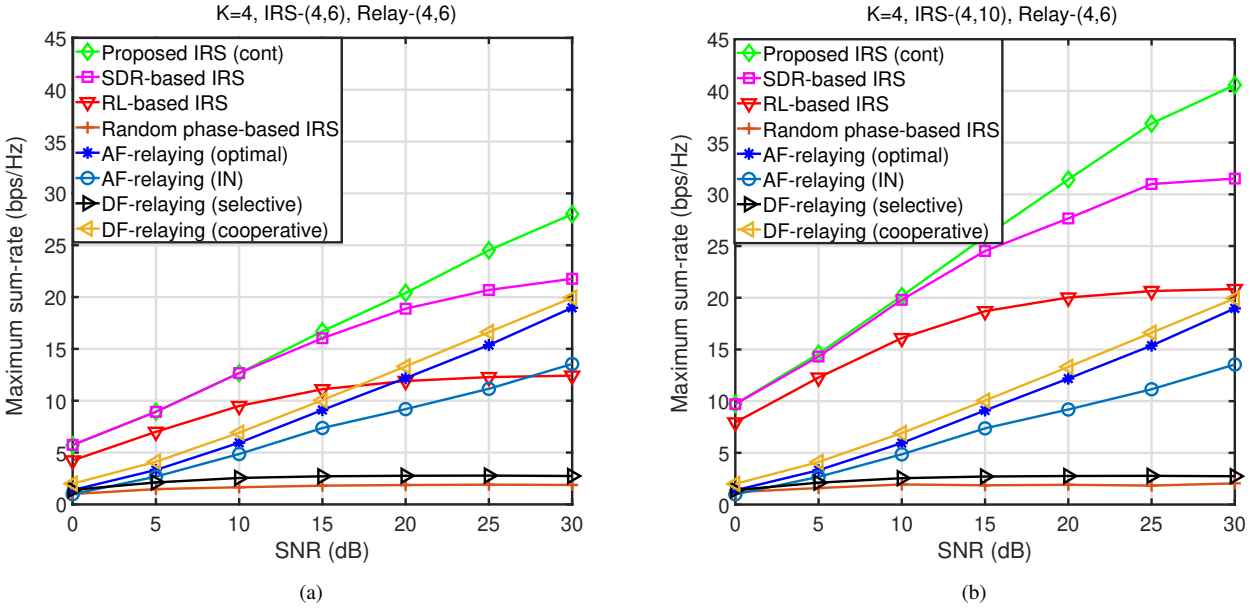

Fig. 4. Maximum sum-rate with $K = 4$ under three settings of IRS and AF/DF relay: **(a)** IRS-(4, 6) and AF/DF relay-(4, 6); **(b)** IRS-(4, 10) and AF/DF relay-(4, 6).

pairs as $K \in \{3, 4\}$, and considered the two settings: i) IRS-(4,6) and AF/DF relay-(4,6); ii) IRS-(4,10) and AF/DF relay-(4,6). In the following, Fig. 3 and Fig. 4 show performance comparison with $K = 3$ and $K = 4$, respectively. First, in Figs. 3(a) and (b), the proposed algorithm provides a higher sum-rate than the compared benchmark schemes over all SNR regions. When we increase the number of IRS elements in each IRS modules as in Fig. 3(b) (satisfying total power budget), the proposed control provides 3%, 3%, 484%, and 588% higher performance than SDR-based IRS, RL-based IRS, DF-relaying (cooperative), and AF-relaying (optimal) at low SNR (around 0 dB) and 16%, 78%, 109%, and 108% gain at high SNR (around 30 dB). The proposed IRS scheme has competitive performance with SDR- and RL-based IRS schemes in low SNR region, but the performance gap increases as SNR becomes higher or the number of IRS elements increases. Second, in Figs. 4(a) and (b), when the number of source-destination pairs increases, the proposed control also achieves the best performance. On the other hand, in Fig. 4(a), we can observe that the proposed control achieves lower sum-rate than that in Fig. 3(a). The reason is that the more user pairs, the more interference, and the IRS only reflects incident signal passively by adjusting its phase shift without actively processing as AF/DF relaying. However,

increasing the number of IRS reflecting elements as in Fig. 4(b) is able to compensate such weakness. In Fig. 4(b), the proposed control provides 0.2%, 23%, 386%, and 605% higher performance than SDR-based IRS, RL-based IRS, DF-relaying (cooperative), and AF-relaying (optimal) at low SNR (around 0 dB) and 29%, 95%, 104%, and 114% gain at high SNR (around 30 dB). Here, comparing Fig. 3, we can see that the performance gap between the proposed scheme and SDR- and RL-based IRS schemes becomes also larger as the number of source-destination pairs increases.

D. Energy Efficiency

1) Power consumption model: In our simulation, we considered power consumption model for the IRS-relaying and conventional relaying systems, i.e., AF and DF relaying. All related parameter values can be referred from Table I. Also, to ensure the fair comparison among those relaying systems, we used the same power budget. For the IRS-based relaying system, the total power consumption consists of transmit power at the sources, the circuit power of all sources and destinations, and the circuit power of all IRSs. Mathematically, the total power consumption can be modeled as [49]:

$$P_{\text{total}}^{\text{IRS}} = \sum_{k=1}^{K}\left(\frac{1}{\nu}p_k + P_{S,k} + P_{D,k}\right) + \sum_{i=1}^{L} M_i P_I, \qquad (69)$$

where ν is the power amplifier efficiency of each source, $P_{S,k}$ and $P_{D,k}$ are the circuit power of k-th source and destination, respectively, and P_I is the circuit power of each IRS element. Next, for the AF-relaying case, we consider L AF relays, where the i-th relay is equipped with M_i antennas. The total power consumption consists of transmit power at the sources (active only half of the time due to half duplexing) and AF relays, the circuit power of all sources and destinations, and the circuit power of all relay antennas. Mathematically, the total power consumption can be modeled as [44]:

$$\begin{aligned} P_{\text{total}}^{\text{AF}} = &\sum_{k=1}^{K}\left(\frac{1}{\nu}p_k + \frac{1}{2}P_{S,k} + P_{D,k}\right) \\ &+ \sum_{i=1}^{L}\left(\frac{1}{\nu_{\text{AF}}}P_{\text{AF},i} + M_i P_{\text{AF}}^{\text{ant}}\right), \end{aligned} \qquad (70)$$

where ν_{AF} is the power amplifier efficiency of each AF relay, $P_{\text{AF},i}$ is the transmit power of the i-th AF relay, and $P_{\text{AF}}^{\text{ant}}$ is the circuit power of each AF-relay antenna. Finally, for the DF-relaying case, we consider transmit power at the sources and each DF relay, the circuit power of all sources and destinations, the circuit power of all relay antennas, and the signal processing power (decode and encode received signal) at the relay. Mathematically, the total power consumption can be modeled as [49]:

$$\begin{aligned} P_{\text{total}}^{\text{DF}} = &\sum_{k=1}^{K}\left(\frac{1}{\nu}p_k + \frac{1}{2}P_{S,k} + P_{D,k}\right) \\ &+ \sum_{i=1}^{L}\left(\frac{1}{\nu_{\text{DF}}}P_{\text{DF},i} + P_{\text{DF},i}^{\text{proc}} + M_i P_{\text{DF}}^{\text{ant}}\right), \end{aligned} \qquad (71)$$

where ν_{DF} is the power amplifier efficiency of each DF relay, $P_{\text{DF},i}$ is the transmit power of the i-th DF relay, $P_{\text{DF},i}^{\text{proc}}$ is the signal processing power of the i-th DF relay, and $P_{\text{DF}}^{\text{ant}}$ is the circuit power of each DF-relay antenna.

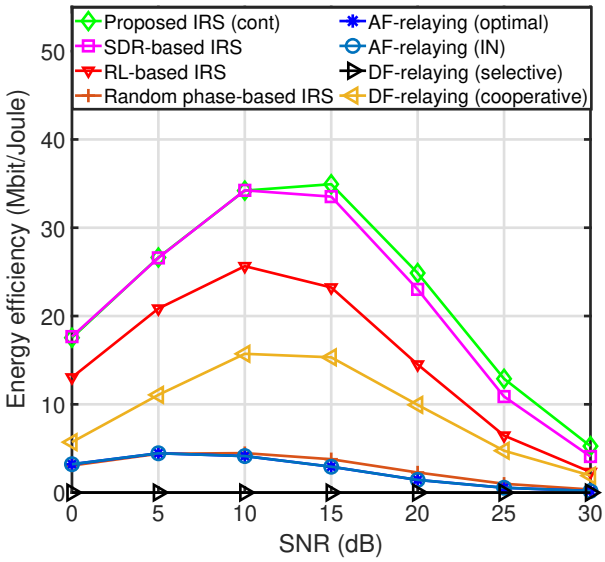

(a)

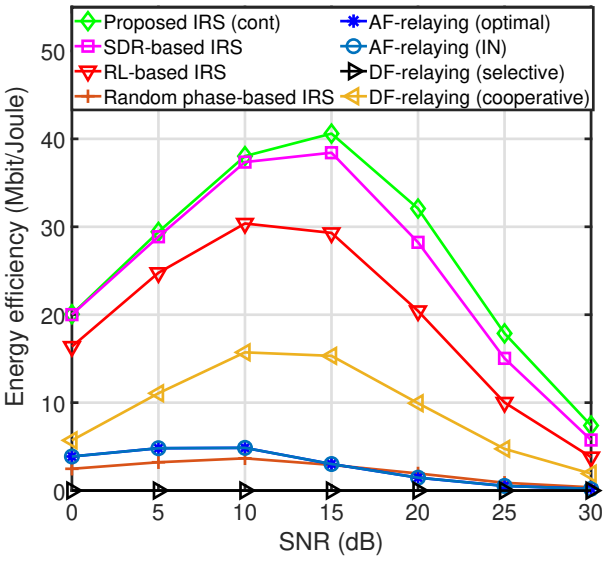

(b)

Fig. 5. Energy efficiency with $K = 4$ under two settings of IRS and AF/DF relay: **(a)** IRS-(4, 6) and AF/DF relay-(4, 6); **(b)** IRS-(4, 10) and AF/DF relay-(4, 6).

2) Results of energy efficiency: In this subsection, we illustrated the achievable energy efficiency (EE) as a function of the SNR in dB. The energy efficiency is defined as $EE = (B \times R)/P_{\text{total}}$, where B is the transmission bandwidth, which is set to 1 (MHz); R is the achievable sum rate at the destinations obtained from subsection IV-C; and P_{total} is the total consumption power of a specific system (IRS-based or AF/DF relaying system), which was modeled in the previous subsection. In this simulation, we used the same settings as

those in subsection IV-C and the number of source-destination pairs is $K = 4$.

As shown in Figs. 5(a) and (b), the energy efficiency of the proposed control is a quasi-concave function of SNR, i.e., increases as the SNR increases within the interval $[0, 15]$ dB, then decreases as SNR is larger than 15 dB. However, the proposed scheme provides higher energy efficiency than the benchmark schemes over all SNR region. Typically, each proposed IRS-(4,6), IRS-(4,10) enhances the energy efficiency by up to 28%, 125%, 207%, 2788% and 29%, 95%, 285%, 3621% compared to SDR-based IRS, RL-based IRS, DF-relaying (cooperative), and AF-relaying (optimal) schemes, respectively. The proposed control's energy efficiency increases as the number of IRS elements increases.

E. Discrete Phase Shift and Imperfect CSI

In this subsection, we evaluate the impact of the discrete phase shift and imperfect CSI on the performance of the proposed algorithm in the sum-rate maximization problem. First, to investigate the effects of discrete value of phase shift, it is practical to consider that $\theta_{i,m}$ can take a discrete value in the set $\mathcal{C} \triangleq \left\{0, \frac{2\pi}{\tau}, \ldots, \frac{2\pi(\tau-1)}{\tau}\right\}$, where $\tau = 2^b$, and b is denoted as the number of bits used to uniformly quantize the continuous phase shift in $[0, 2\pi)$. The quantized solution $\tilde{\theta}_{i,m}$ is then obtained as

$$\tilde{\theta}_{i,m} = \arg\min_{\theta \in \mathcal{D}} |e^{j\theta} - \phi^{\star}_{i,m}|, \forall m \in \{1, ..., M_i\}, \forall i \in \mathcal{L} \quad (72)$$

by mapping the obtained solution $\boldsymbol{\phi}^{\star}_{i,m}$ to the nearest value in set $\mathcal{C}$. For the discrete case of the IRS-based system, we considered 3-bit phase shifters, which is known to be an efficient number of bits providing less performance degradation with fewer bits [50], [51]. As shown in Fig. 6, when the quantized discrete control is applied, the maximum loss of performance gain for two cases (a) and (b) are 33%, 29%, respectively. However, the performance gap between the proposed continuous control and the discrete approximation based controls becomes smaller, as the SNR decreases or the number of IRS element increases. In low SNR region, the discrete phase approximation can achieve near-optimal performance.

Next, we investigate the effects of the imperfect CSI in our proposed IRS-based performance. Following [52], the estimated channel for $\boldsymbol{e}_{i,k}$ is modeled as $\hat{\boldsymbol{e}}_{i,k} = \sqrt{1-\delta}\boldsymbol{e}_{i,k} + \sqrt{\delta}\triangle\boldsymbol{e}_{i,k}$, where $\delta \in [0, 1]$ is the level of reliability of the estimation, $\triangle\boldsymbol{e}_{i,k} \sim \mathcal{CN}(0, \sigma^2_{\triangle\boldsymbol{e}_{i,k}}\boldsymbol{I})$ is the estimation error, with $\sigma^2_{\triangle\boldsymbol{e}_{i,k}}$ is the error variance of channel estimation. Similarly, the estimated channel for $\boldsymbol{f}_{k,i}$ are also modeled as $\hat{\boldsymbol{f}}_{k,i} = \sqrt{1-\delta}\boldsymbol{f}_{k,i} + \sqrt{\delta}\triangle\boldsymbol{f}_{k,i}$. As shown in Figs. 6(a), and (b), the performance gap between the proposed control and imperfect CSI based control becomes smaller with lower value of δ, i.e., maximally 4.3% and 17.3% degradation for $\delta = 0.1$ and $\delta = 0.5$, respectively. The same observation holds for the discrete phase approximation of the proposed control, i.e., maximally, 4% and 17.2% degradation for $\delta = 0.1$ and $\delta = 0.5$, respectively.

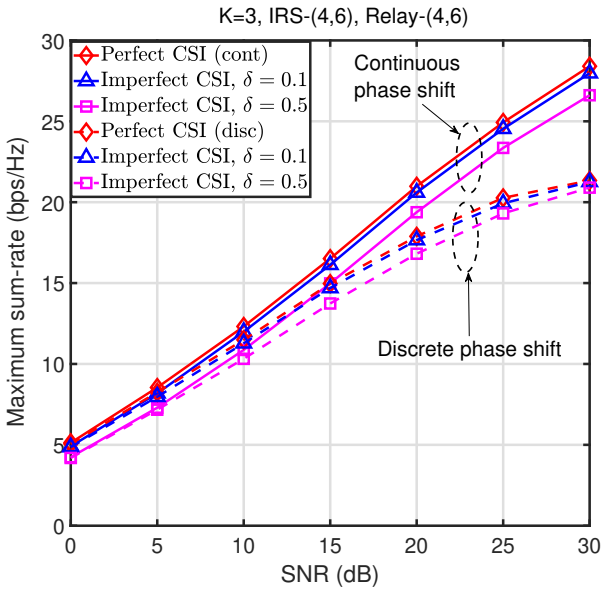

(a)

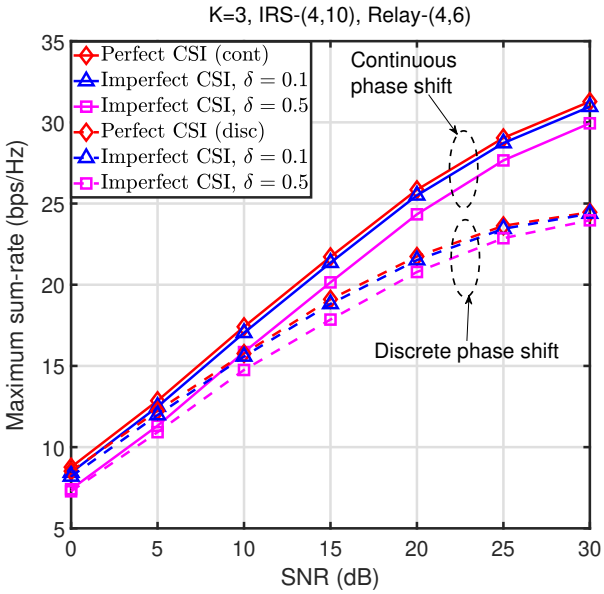

(b)

Fig. 6. The effects of imperfect CSI and discrete phase shift with $K = 3$: (a) IRS-(4,6) and relay-(4,6); (b) IRS-(4,10) and relay-(4,6).

V. Conclusions

In this paper, we proposed optimal distributed IRS controls for a multi-hop interference channel. We first identified the achievable rate region of two-hop coordinated IRS relaying network using the proposed SCA approach. Then, we found maximum sum-rate using the proposed AO and ADMM based distributed IRS control, and proved its convergence and optimality. Finally, we demonstrated that the proposed controls provide higher performance than SDR-, random-phase-, DRL-based IRS controls and AF-, DF-, IN-based relaying controls, in terms of achievable rate region, achievable sum-rate, and energy efficiency. We also confirmed that the discrete phase approximation of the proposed control provides near-optimal

performance with fewer bits, and the proposed control is robust under imperfect CSI condition. The proposed controls can be efficiently applied to large-scale multi-pair multihop device-to-device (D2D) and machine-type device communications in interference-limited or low-powered dense networks of 5G and 6G environments. In future studies, we will investigate distributed hybrid models that exploit various multi-antenna relaying schemes and the proposed IRS control opportunistically or jointly under practical channel conditions in various multi-hop environments.

APPENDIX A
PROOF OF PROPOSITION 1

Proof. (a) The desired signal power, i.e., $\mathbb{E}[|y_{S,k}|^2]$, is decomposed as follows:

$$\begin{aligned}
P_{S,k} &= \mathbb{E}[|y_{S,k}|^2] = \mathbb{E}\left[\left|\sum_{i=1}^{L}\sqrt{p_k}\boldsymbol{f}_{k,i}^T\boldsymbol{\Phi}_i\boldsymbol{e}_{i,k}s_k\right|^2\right] \\
&= p_k\mathbb{E}\left[\left(\sum_{i=1}^{L}\boldsymbol{f}_{k,i}^T\boldsymbol{\Phi}_i\boldsymbol{e}_{i,k}s_k\right)\left(\sum_{i=1}^{L}\boldsymbol{f}_{k,i}^T\boldsymbol{\Phi}_i\boldsymbol{e}_{i,k}s_k\right)^H\right] \\
&\overset{(1)}{=} p_k\left(\sum_{i=1}^{L}\boldsymbol{f}_{k,i}^T\boldsymbol{\Phi}_i\boldsymbol{e}_{i,k}\right)\underbrace{\mathbb{E}[s_ks_k^H]}_{=1}\left(\sum_{i=1}^{L}\boldsymbol{f}_{k,i}^T\boldsymbol{\Phi}_i\boldsymbol{e}_{i,k}\right)^H \\
&= p_k\text{tr}\left(\left(\sum_{i=1}^{L}\boldsymbol{f}_{k,i}^T\boldsymbol{\Phi}_i\boldsymbol{e}_{i,k}\right)\left(\sum_{i=1}^{L}\boldsymbol{f}_{k,i}^T\boldsymbol{\Phi}_i\boldsymbol{e}_{i,k}\right)^H\right) \\
&\overset{(2)}{=} p_k\left(\text{Vec}\left(\sum_{i=1}^{L}\boldsymbol{f}_{k,i}^T\boldsymbol{\Phi}_i\boldsymbol{e}_{i,k}\right)^*\right)^T\text{Vec}\left(\sum_{i=1}^{L}\boldsymbol{f}_{k,i}^T\boldsymbol{\Phi}_i\boldsymbol{e}_{i,k}\right) \\
&= p_k\left(\sum_{i=1}^{L}\text{Vec}\left(\boldsymbol{f}_{k,i}^T\boldsymbol{\Phi}_i\boldsymbol{e}_{i,k}\right)\right)^H\sum_{i=1}^{L}\text{Vec}\left(\boldsymbol{f}_{k,i}^T\boldsymbol{\Phi}_i\boldsymbol{e}_{i,k}\right) \\
&\overset{(3)}{=} p_k\sum_{i=1}^{L}(\text{diag}(\boldsymbol{\Phi}_i))^H\left(\boldsymbol{e}_{i,k}^T*\boldsymbol{f}_{k,i}^T\right)^H\sum_{i=1}^{L}\left(\boldsymbol{e}_{i,k}^T*\boldsymbol{f}_{k,i}^T\right) \\
&\qquad\qquad\times\text{diag}(\boldsymbol{\Phi}_i) \\
&= p_k\sum_{i=1}^{L}\boldsymbol{\phi}_i^H\left(\boldsymbol{e}_{i,k}^T*\boldsymbol{f}_{k,i}^T\right)^H\sum_{i=1}^{L}\left(\boldsymbol{e}_{i,k}^T*\boldsymbol{f}_{k,i}^T\right)\boldsymbol{\phi}_i \\
&= p_k(\boldsymbol{\phi}^H\boldsymbol{S}_k\boldsymbol{\phi}),
\end{aligned}$$

where $\boldsymbol{\phi}_i = \text{diag}(\boldsymbol{\Phi}_i)$[1], $\boldsymbol{\phi} = \left[\boldsymbol{\phi}_1^T,\ldots,\boldsymbol{\phi}_L^T\right]^T$, $\boldsymbol{a}_k = \left[\left(\boldsymbol{e}_{1,k}^T*\boldsymbol{f}_{k,1}^T\right),\ldots,\left(\boldsymbol{e}_{L,k}^T*\boldsymbol{f}_{k,L}^T\right)\right]^H$, and $\boldsymbol{S}_k = \boldsymbol{a}_k\boldsymbol{a}_k^H$.

In the above decomposition, (1) is due to the fact that $s_k \sim \mathcal{CN}(0,1), \forall k$ are independent from each other; (2) is obtained by applying $\text{Tr}(\boldsymbol{AB}) = \left(\text{Vec}(\boldsymbol{B}^T)\right)^T\text{Vec}(\boldsymbol{A})$; and (3) is obtained by applying $\text{Vec}(\boldsymbol{ABC}) = \left(\boldsymbol{C}^T*\boldsymbol{A}\right)\text{diag}(\boldsymbol{B})$ [53].

[1]$\text{diag}(\boldsymbol{A}) = [a_{11},...,a_{nn}]^T$, where a_{ii} are the diagonal entries of an $n\times n$ matrix $\boldsymbol{A}$.

(b) Similarly, by applying the same identities as in (a), the interference signal power is decomposed as follows:

$$\begin{aligned}
P_{I,k} &= \mathbb{E}[|y_{I,k}|^2] = \mathbb{E}\left[\left|\sum_{i=1}^{L}\boldsymbol{f}_{k,i}^T\boldsymbol{\Phi}_i\bar{\boldsymbol{E}}_{i,k}\bar{\boldsymbol{P}}_k^{\frac{1}{2}}\bar{\boldsymbol{s}}_k\right|^2\right] \\
&= \mathbb{E}\left[\left(\sum_{i=1}^{L}\boldsymbol{f}_{k,i}^T\boldsymbol{\Phi}_i\bar{\boldsymbol{E}}_{i,k}\bar{\boldsymbol{P}}_k^{\frac{1}{2}}\bar{\boldsymbol{s}}_k\right)\left(\sum_{i=1}^{L}\boldsymbol{f}_{k,i}^T\boldsymbol{\Phi}_i\bar{\boldsymbol{E}}_{i,k}\bar{\boldsymbol{P}}_k^{\frac{1}{2}}\bar{\boldsymbol{s}}_k\right)^H\right] \\
&\overset{(1)}{=} \left(\sum_{i=1}^{L}\boldsymbol{f}_{k,i}^T\boldsymbol{\Phi}_i\bar{\boldsymbol{E}}_{i,k}\bar{\boldsymbol{P}}_k^{\frac{1}{2}}\right)\underbrace{\mathbb{E}\left[\bar{\boldsymbol{s}}_k\bar{\boldsymbol{s}}_k^H\right]}_{=\boldsymbol{I}_{K-1}}\left(\sum_{i=1}^{L}\boldsymbol{f}_{k,i}^T\boldsymbol{\Phi}_i\bar{\boldsymbol{E}}_{i,k}\bar{\boldsymbol{P}}_k^{\frac{1}{2}}\right)^H \\
&= \text{tr}\left(\left(\sum_{i=1}^{L}\boldsymbol{f}_{k,i}^T\boldsymbol{\Phi}_i\bar{\boldsymbol{E}}_{i,k}\bar{\boldsymbol{P}}_k^{\frac{1}{2}}\right)\left(\sum_{i=1}^{L}\boldsymbol{f}_{k,i}^T\boldsymbol{\Phi}_i\bar{\boldsymbol{E}}_{i,k}\bar{\boldsymbol{P}}_k^{\frac{1}{2}}\right)^H\right) \\
&= \left(\text{Vec}\left(\sum_{i=1}^{L}\boldsymbol{f}_{k,i}^T\boldsymbol{\Phi}_i\bar{\boldsymbol{E}}_{i,k}\bar{\boldsymbol{P}}_k^{\frac{1}{2}}\right)^*\right)^T \\
&\qquad\times\text{Vec}\left(\sum_{i=1}^{L}\boldsymbol{f}_{k,i}^T\boldsymbol{\Phi}_i\bar{\boldsymbol{E}}_{i,k}\bar{\boldsymbol{P}}_k^{\frac{1}{2}}\right) \\
&= \sum_{i=1}^{L}(\text{diag}(\boldsymbol{\Phi}_i))^H\left(\left(\bar{\boldsymbol{E}}_{i,k}\bar{\boldsymbol{P}}_k^{\frac{1}{2}}\right)^T*\boldsymbol{f}_{k,i}^T\right)^H \\
&\qquad\times\sum_{i=1}^{L}\left(\left(\bar{\boldsymbol{E}}_{i,k}\bar{\boldsymbol{P}}_k^{\frac{1}{2}}\right)^T*\boldsymbol{f}_{k,i}^T\right)\text{diag}(\boldsymbol{\Phi}_i) \\
&= \boldsymbol{\phi}^H\boldsymbol{K}_k\boldsymbol{\phi},
\end{aligned}$$

where $\boldsymbol{B}_k = \left[\left(\bar{\boldsymbol{E}}_{1,k}\bar{\boldsymbol{P}}_k^{\frac{1}{2}}\right)^T*\boldsymbol{f}_{k,1}^T,...,\left(\bar{\boldsymbol{E}}_{L,k}\bar{\boldsymbol{P}}_k^{\frac{1}{2}}\right)^T*\boldsymbol{f}_{k,L}^T\right]$, and $\boldsymbol{K}_k = \boldsymbol{B}_k^H\boldsymbol{B}_k$. In the above decomposition, (1) is due to the fact that $\bar{\boldsymbol{s}}_k = [s_1,...,s_{k-1},s_{k+1},...,s_K]^T$, where $s_k \sim \mathcal{CN}(0,1), \forall k$ are independent from each other. This completes the proof of Proposition 1. □

APPENDIX B
PROOF OF STRONG CONCAVITY OF $\mathcal{L}_\rho(\boldsymbol{\varphi}^{t+1},\boldsymbol{\phi},\boldsymbol{\lambda}^t)$

Proof. For the sake of simplicity, let $\bar{\boldsymbol{\varphi}} \triangleq \boldsymbol{\varphi}^{t+1}, \bar{\boldsymbol{\lambda}} \triangleq \boldsymbol{\lambda}^t$. We prove that for the given $\bar{\boldsymbol{\varphi}},\bar{\boldsymbol{\lambda}}$, the function $g(\boldsymbol{\phi}) \triangleq -\mathcal{L}_\rho(\bar{\boldsymbol{\varphi}},\boldsymbol{\phi},\bar{\boldsymbol{\lambda}})$ is strongly convex. Indeed, we have

$$\begin{aligned}
g(\boldsymbol{\phi}) &= \boldsymbol{\phi}^H\boldsymbol{A}\boldsymbol{\phi} - \text{Re}\{\boldsymbol{a}^H\boldsymbol{\phi}\} + \iota_{\mathcal{F}}(\bar{\boldsymbol{\varphi}}) - \text{Re}\{\bar{\boldsymbol{\lambda}}^H(\bar{\boldsymbol{\varphi}}-\boldsymbol{\phi})\} \\
&\quad + \frac{\rho}{2}\|\bar{\boldsymbol{\varphi}}-\boldsymbol{\phi}\|_2^2 \\
&= \boldsymbol{\phi}^H\bar{\boldsymbol{A}}\boldsymbol{\phi} - \text{Re}\{\bar{\boldsymbol{a}}^H\boldsymbol{\phi}\} + c,
\end{aligned} \tag{73}$$

where $\bar{\boldsymbol{A}} \triangleq \boldsymbol{A} + \frac{\rho}{2}\boldsymbol{I}, \bar{\boldsymbol{a}} \triangleq \boldsymbol{a} - \rho\bar{\boldsymbol{\varphi}} + \bar{\boldsymbol{\lambda}}$, and $c \triangleq \frac{\rho}{2}\bar{\boldsymbol{\varphi}}^H\bar{\boldsymbol{\varphi}} + \iota_{\mathcal{F}}(\bar{\boldsymbol{\varphi}}) - \text{Re}\{\bar{\boldsymbol{\lambda}}^H\bar{\boldsymbol{\varphi}}\}$. For $\boldsymbol{\varphi_1},\boldsymbol{\varphi_2} \in \mathbb{C}^{\sum_{i=1}^{L}M_i\times 1}, \boldsymbol{\gamma_1},\boldsymbol{\gamma_2} \in [0,1], \boldsymbol{\gamma_1}+\boldsymbol{\gamma_2}=1$, we have

$$\begin{aligned}
g(\boldsymbol{\gamma_1}\boldsymbol{\phi_1}+\boldsymbol{\gamma_2}\boldsymbol{\phi_2}) &= (\boldsymbol{\gamma_1}\boldsymbol{\phi_1}+\boldsymbol{\gamma_2}\boldsymbol{\phi_2})^H\bar{\boldsymbol{A}}(\boldsymbol{\gamma_1}\boldsymbol{\phi_1}+\boldsymbol{\gamma_2}\boldsymbol{\phi_2}) \\
&\quad - \text{Re}\{\bar{\boldsymbol{a}}^H(\boldsymbol{\gamma_1}\boldsymbol{\phi_1}+\boldsymbol{\gamma_2}\boldsymbol{\phi_2})\} + c \\
&\le \boldsymbol{\gamma_1}g(\boldsymbol{\gamma_1}) + \boldsymbol{\gamma_2}g(\boldsymbol{\gamma_2}) - \frac{\rho}{2}\boldsymbol{\gamma_1}\boldsymbol{\gamma_2}\|\boldsymbol{\phi_1}-\boldsymbol{\phi_2}\|_2^2.
\end{aligned} \tag{74}$$

The last inequality holds because of using $\bar{\boldsymbol{A}} = \boldsymbol{A} + \frac{\rho}{2}\boldsymbol{I}$, and based on the fact that $\boldsymbol{A}$ is positive semidefinite, we obtain the following:

$$\begin{aligned}&\boldsymbol{\phi_1}^H \bar{\boldsymbol{A}}\boldsymbol{\phi_1} + \boldsymbol{\phi_2}^H \bar{\boldsymbol{A}}\boldsymbol{\phi_2} - \boldsymbol{\phi_1}^H \bar{\boldsymbol{A}}\boldsymbol{\phi_2} - \boldsymbol{\phi_2}^H \bar{\boldsymbol{A}}\boldsymbol{\phi_1} \\ &\quad = (\boldsymbol{\phi_1} - \boldsymbol{\phi_2})^H \boldsymbol{A}(\boldsymbol{\phi_1} - \boldsymbol{\phi_2}) + \frac{\rho}{2}\|\boldsymbol{\phi_1} - \boldsymbol{\phi_2}\|_2^2 \\ &\quad \geq \frac{\rho}{2}\|\boldsymbol{\phi_1} - \boldsymbol{\phi_2}\|_2^2.\end{aligned} \tag{75}$$

The inequality in (74) implies that

$$\begin{aligned}g(\boldsymbol{\gamma_1}\boldsymbol{\phi_1} + \boldsymbol{\gamma_2}\boldsymbol{\phi_2}) \leq \boldsymbol{\gamma_1} g(\boldsymbol{\gamma_1}) + \boldsymbol{\gamma_2} g(\boldsymbol{\gamma_2}) \\ - \frac{\rho}{2}\boldsymbol{\gamma_1}\boldsymbol{\gamma_2}\|\boldsymbol{\phi_1} - \boldsymbol{\phi_2}\|_2^2,\end{aligned} \tag{76}$$

which means that $g(\boldsymbol{\phi})$ is strongly convex, or equivalently, the function $\mathcal{L}_\rho(\boldsymbol{\varphi}^{t+1}, \boldsymbol{\phi}, \boldsymbol{\lambda}^t)$ is strongly concave. This completes the proof. □

REFERENCES

[1] Y. Liu, X. Liu, X. Mu, T. Hou, J. Xu, M. D. Renzo, and N. Al-Dhahir, "Reconfigurable intelligent surfaces: Principles and opportunities," 2021.

[2] L. Dai, B. Wang, M. Wang, X. Yang, J. Tan, S. Bi, S. Xu, F. Yang, Z. Chen, M. Di Renzo *et al.*, "Reconfigurable intelligent surface-based wireless communications: Antenna design, prototyping, and experimental results," *IEEE Access*, vol. 8, pp. 45 913–45 923, 2020.

[3] C. Huang, S. Hu, G. C. Alexandropoulos, A. Zappone, C. Yuen, R. Zhang, M. Di Renzo, and M. Debbah, "Holographic mimo surfaces for 6g wireless networks: Opportunities, challenges, and trends," *IEEE Wireless Communications*, vol. 27, no. 5, pp. 118–125, 2020.

[4] M. Di Renzo, A. Zappone, M. Debbah, M.-S. Alouini, C. Yuen, J. de Rosny, and S. Tretyakov, "Smart radio environments empowered by reconfigurable intelligent surfaces: How it works, state of research, and the road ahead," *IEEE Journal on Selected Areas in Communications*, vol. 38, no. 11, pp. 2450–2525, 2020.

[5] M. Di Renzo, M. Debbah, D.-T. Phan-Huy, A. Zappone, M.-S. Alouini, C. Yuen, V. Sciancalepore, G. C. Alexandropoulos, J. Hoydis, H. Gacanin *et al.*, "Smart radio environments empowered by reconfigurable ai meta-surfaces: An idea whose time has come," *EURASIP Journal on Wireless Communications and Networking*, vol. 2019, no. 1, pp. 1–20, 2019.

[6] A. Welkie, L. Shangguan, J. Gummeson, W. Hu, and K. Jamieson, "Programmable radio environments for smart spaces," in *Proceedings of the 16th ACM Workshop on Hot Topics in Networks*, 2017, pp. 36–42.

[7] C. Liaskos, S. Nie, A. Tsioliaridou, A. Pitsillides, S. Ioannidis, and I. Akyildiz, "A novel communication paradigm for high capacity and security via programmable indoor wireless environments in next generation wireless systems," *Ad Hoc Networks*, vol. 87, pp. 1–16, 2019.

[8] J. Zhang, Y. Zhang, C. Zhong, and Z. Zhang, "Robust design for intelligent reflecting surfaces assisted miso systems," *IEEE Communications Letters*, vol. 24, no. 10, pp. 2353–2357, 2020.

[9] Q. Wu and R. Zhang, "Intelligent reflecting surface enhanced wireless network: Joint active and passive beamforming design," in *2018 IEEE Global Communications Conference (GLOBECOM)*, 2018, pp. 1–6.

[10] H. Guo, Y.-C. Liang, J. Chen, and E. G. Larsson, "Weighted sum-rate maximization for intelligent reflecting surface enhanced wireless networks," in *2019 IEEE Global Communications Conference (GLOBECOM)*, 2019, pp. 1–6.

[11] S. Zhang and R. Zhang, "Capacity characterization for intelligent reflecting surface aided mimo communication," *IEEE Journal on Selected Areas in Communications*, vol. 38, no. 8, pp. 1823–1838, 2020.

[12] N. S. Perović, L.-N. Tran, M. Di Renzo, and M. F. Flanagan, "Achievable rate optimization for mimo systems with reconfigurable intelligent surfaces," *IEEE Transactions on Wireless Communications*, pp. 3865–3882, 2021.

[13] Z. Yang, M. Chen, W. Saad, W. Xu, M. Shikh-Bahaei, H. V. Poor, and S. Cui, "Energy-efficient wireless communications with distributed reconfigurable intelligent surfaces," *IEEE Transactions on Wireless Communications*, 2021.

[14] K.-W. Huang and H.-M. Wang, "Passive beamforming for irs aided wireless networks," *IEEE Wireless Communications Letters*, vol. 9, no. 12, pp. 2035–2039, 2020.

[15] W. Huang, Y. Zeng, and Y. Huang, "Achievable rate region of miso interference channel aided by intelligent reflecting surface," *IEEE Transactions on Vehicular Technology*, vol. 69, no. 12, pp. 16 264–16 269, 2020.

[16] Z. Zhang and L. Dai, "Capacity improvement in wideband reconfigurable intelligent surface-aided cell-free network," in *2020 IEEE 21st International Workshop on Signal Processing Advances in Wireless Communications (SPAWC)*, 2020, pp. 1–5.

[17] S. Huang, Y. Ye, M. Xiao, H. V. Poor, and M. Skoglund, "Decentralized beamforming design for intelligent reflecting surface-enhanced cell-free networks," *IEEE Wireless Communications Letters*, vol. 10, no. 3, pp. 673–677, 2020.

[18] M. Hua, Q. Wu, D. W. K. Ng, J. Zhao, and L. Yang, "Intelligent reflecting surface-aided joint processing coordinated multipoint transmission," *IEEE Transactions on Communications*, vol. 69, no. 3, pp. 1650–1665, 2021.

[19] A. H. A. Bafghi, V. Jamali, M. Nasiri-Kenari, and R. Schober, "Degrees of freedom of the k-user interference channel in the presence of intelligent reflecting surfaces," *arXiv preprint arXiv:2012.13787*, 2020.

[20] Z. Peng, T. Li, C. Pan, H. Ren, W. Xu, and M. Di Renzo, "Analysis and optimization for ris-aided multi-pair communications relying on statistical csi," *IEEE Transactions on Vehicular Technology*, vol. 70, no. 4, pp. 3897–3901, 2021.

[21] L. Yang, Y. Yang, D. B. d. Costa, and I. Trigui, "Outage probability and capacity scaling law of multiple ris-aided networks," *IEEE Wireless Communications Letters*, vol. 10, no. 2, pp. 256–260, 2021.

[22] H. Du, J. Zhang, J. Cheng, and B. Ai, "Millimeter wave communications with reconfigurable intelligent surfaces: Performance analysis and optimization," *IEEE Transactions on Communications*, vol. 69, no. 4, pp. 2752–2768, 2021.

[23] J. He, K. Yu, and Y. Shi, "Coordinated passive beamforming for distributed intelligent reflecting surfaces network," in *2020 IEEE 91st Vehicular Technology Conference (VTC2020-Spring)*, 2020, pp. 1–5.

[24] M. Zeng, E. Bedeer, O. A. Dobre, P. Fortier, Q.-V. Pham, and W. Hao, "Energy-efficient resource allocation for irs-assisted multi-antenna uplink systems," *IEEE Wireless Communications Letters*, 2021.

[25] G. Zhu, Y. Wang, and K. Huang, "Broadband analog aggregation for low-latency federated edge learning," *IEEE Transactions on Wireless Communications*, vol. 19, no. 1, pp. 491–506, 2019.

[26] J. Yuan, Y.-C. Liang, J. Joung, G. Feng, and E. G. Larsson, "Intelligent reflecting surface-assisted cognitive radio system," *IEEE Transactions on Communications*, vol. 69, no. 1, pp. 675–687, 2020.

[27] H. Alwazani, A. Kammoun, A. Chaaban, M. Debbah, M.-S. Alouini *et al.*, "Intelligent reflecting surface-assisted multi-user miso communication: Channel estimation and beamforming design," *IEEE Open Journal of the Communications Society*, vol. 1, pp. 661–680, 2020.

[28] Z. Wang, L. Liu, and S. Cui, "Channel estimation for intelligent reflecting surface assisted multiuser communications: Framework, algorithms, and analysis," *IEEE Transactions on Wireless Communications*, vol. 19, no. 10, pp. 6607–6620, 2020.

[29] P. Wang, J. Fang, H. Duan, and H. Li, "Compressed channel estimation for intelligent reflecting surface-assisted millimeter wave systems," *IEEE Signal Processing Letters*, vol. 27, pp. 905–909, 2020.

[30] Y. Cui and H. Yin, "An efficient csi acquisition method for intelligent reflecting surface-assisted mmwave networks," *arXiv preprint arXiv:1912.12076*, 2019.

[31] B. Zheng, C. You, and R. Zhang, "Fast channel estimation for irs-assisted ofdm," *IEEE Wireless Communications Letters*, vol. 10, no. 3, pp. 580–584, 2021.

[32] Z. Huang, B. Zheng, and R. Zhang, "Transforming fading channel from fast to slow: Irs-assisted high-mobility communication," in *ICC 2021 - IEEE International Conference on Communications*, 2021, pp. 1–6.

[33] R. Zhang and S. Cui, "Cooperative interference management with miso beamforming," *IEEE Transactions on Signal Processing*, vol. 58, no. 10, pp. 5450–5458, 2010.

[34] H. Xie, J. Xu, and Y.-F. Liu, "Max-min fairness in irs-aided multi-cell miso systems with joint transmit and reflective beamforming," *IEEE Transactions on Wireless Communications*, vol. 20, no. 2, pp. 1379–1393, 2020.

[35] M. Grant and S. Boyd, "CVX: Matlab software for disciplined convex programming, version 2.1," http://cvxr.com/cvx, Mar. 2014.

[36] K. Shen and W. Yu, "Fractional programming for communication systems—part ii: Uplink scheduling via matching," *IEEE Transactions on Signal Processing*, vol. 66, no. 10, pp. 2631–2644, 2018.

[37] S. Boyd, N. Parikh, and E. Chu, *Distributed optimization and statistical learning via the alternating direction method of multipliers*. Now Publishers Inc, 2011.

[38] Y. Wang, W. Yin, and J. Zeng, "Global convergence of admm in nonconvex nonsmooth optimization," *Journal of Scientific Computing*, vol. 78, no. 1, pp. 29–63, 2019.

[39] H. Guo, Y.-C. Liang, J. Chen, and E. G. Larsson, "Weighted sum-rate optimization for intelligent reflecting surface enhanced wireless networks," *arXiv preprint arXiv:1905.07920*, 2019.

[40] Q. Li, C. Li, and J. Lin, "Constant modulus secure beamforming for multicast massive mimo wiretap channels," *IEEE Transactions on Information Forensics and Security*, vol. 15, pp. 264–275, 2019.

[41] Y. Nesterov, *Introductory lectures on convex optimization: A basic course*. Springer Science & Business Media, 2003, vol. 87.

[42] Y. Cao, T. Lv, W. Ni, and Z. Lin, "Sum-rate maximization for multi-reconfigurable intelligent surface-assisted device-to-device communications," *IEEE Transactions on Communications*, 2021.

[43] A. Ben-Tal and A. Nemirovski, *Lectures on modern convex optimization: analysis, algorithms, and engineering applications*. SIAM, 2001.

[44] C. Huang, A. Zappone, G. C. Alexandropoulos, M. Debbah, and C. Yuen, "Reconfigurable intelligent surfaces for energy efficiency in wireless communication," *IEEE Transactions on Wireless Communications*, vol. 18, no. 8, pp. 4157–4170, 2019.

[45] Z. Yang, M. Chen, W. Saad, W. Xu, M. Shikh-Bahaei, H. V. Poor, and S. Cui, "Energy-efficient wireless communications with distributed reconfigurable intelligent surfaces," *IEEE Transactions on Wireless Communications*, 2021.

[46] Q. Wu and R. Zhang, "Intelligent reflecting surface enhanced wireless network via joint active and passive beamforming," *IEEE Transactions on Wireless Communications*, vol. 18, no. 11, pp. 5394–5409, 2019.

[47] C. Huang, R. Mo, and C. Yuen, "Reconfigurable intelligent surface assisted multiuser miso systems exploiting deep reinforcement learning," *IEEE Journal on Selected Areas in Communications*, vol. 38, no. 8, pp. 1839–1850, 2020.

[48] Y. Shi, J. Zhang, and K. B. Letaief, "Coordinated relay beamforming for amplify-and-forward two-hop interference networks," in *2012 IEEE Global Communications Conference (GLOBECOM)*, 2012, pp. 2408–2413.

[49] E. Björnson, Ö. Özdogan, and E. G. Larsson, "Intelligent reflecting surface versus decode-and-forward: How large surfaces are needed to beat relaying?" *IEEE Wireless Communications Letters*, vol. 9, no. 2, pp. 244–248, 2019.

[50] H. Xie, J. Xu, and Y.-F. Liu, "Max-min fairness in irs-aided multi-cell miso systems with joint transmit and reflective beamforming," *IEEE Transactions on Wireless Communications*, 2020.

[51] X. Mu, Y. Liu, L. Guo, J. Lin, and R. Schober, "Intelligent reflecting surface enhanced indoor robot path planning: A radio map based approach," *IEEE Transactions on Wireless Communications*, 2021.

[52] Y. Gao, C. Yong, Z. Xiong, J. Zhao, Y. Xiao, and D. Niyato, "Reflection resource management for intelligent reflecting surface aided wireless networks," *IEEE Transactions on Communications*, vol. 69, no. 10, pp. 6971–6986, 2021.

[53] X.-D. Zhang, *Matrix analysis and applications*. Cambridge University Press, 2017.

The Vi Nguyen received the B.S. degree in Mathematics from University of Science, Ho Chi Minh City, Viet Nam in 2016, and M.S. degree in Computer Science and Engineering from Chung-Ang University, South Korea in 2021. He is currently pursuing Ph.D. in Big Data at Chung-Ang University, South Korea. His research interests include machine learning, optimization, and their applications in wireless communications.

Thanh Phung Truong received the B.S. degree in Electronics-Telecommunications Engineering from Ho Chi Minh City University of Technology, Vietnam, in 2018, and M.S. degree in Computer Science and Engineering from Chung-Ang University, South Korea, in 2022. His research interests include machine learning, mobile edge computing, and wireless communication.

Thi My Tuyen Nguyen received the B.S. degree in Mathematics from University of Science, Ho Chi Minh City, Viet Nam in 2016, and M.S. degree in Computer Science and Engineering from Soongsil University, South Korea in 2021. She is currently pursuing Ph.D. in Big Data at Chung-Ang University, South Korea. Her research interests include machine learning, optimization, and their applications in wireless communications.

Wonjong Noh received the B.S., M.S., and Ph.D. degrees from the Department of Electronics Engineering, Korea University, Seoul, South Korea, in 1998, 2000, and 2005, respectively. From 2005 to 2007, he conducted the Postdoctoral Research with Purdue University, West Lafayette, IN, USA, and the University of California at Irvine, Irvine, CA, USA. From 2008 to 2015, he was a Principal Research Engineer with the Samsung Advanced Institute of Technology, Samsung Electronics, South Korea. After that, he worked as an Assistant Professor with the Department of Electronics and Communication Engineering, Gyeonggi University of Science and Technology, South Korea, and since 2019, he is working as an Associate Professor with the School of Software, Hallym University, South Korea. He received the Government Postdoctoral Fellowship from the Ministry of Information and Communication, South Korea, in 2005. He was also a recipient of the Samsung Best Paper Gold Award in 2010, the Samsung Patent Bronze Award in 2011, and the Samsung Technology Award in 2013. His current research interests include fundamental analysis and evaluations on machine learning-based 5G and 6G wireless communications and networks.

Sungrae Cho received B.S. and M.S. degrees in Electronics Engineering from Korea University, Seoul, South Korea, in 1992 and 1994, respectively, and Ph.D. degree in Electrical and Computer Engineering from the Georgia Institute of Technology, Atlanta, GA, USA, in 2002. He is a Professor with the School of Computer Science and Engineering, Chung-Ang University (CAU), Seoul, South Korea. Prior to joining CAU, he was an Assistant Professor with the Department of Computer Sciences, Georgia Southern University, Statesboro, GA, USA, from 2003 to 2006, and a Senior Member of Technical Staff with the Samsung Advanced Institute of Technology (SAIT), Kiheung, South Korea, in 2003. From 1994 to 1996, he was a Research Staff Member with Electronics and Telecommunications Research Institute (ETRI), Daejeon, South Korea. From 2012 to 2013, he held a Visiting Professorship with the National Institute of Standards and Technology (NIST), Gaithersburg, MD, USA. His current research interests include wireless networking, ubiquitous computing, and ICT convergence. He has been a Subject Editor of IET Electronics Letter since 2018, and was an Area Editor of Ad Hoc Networks Journal (Elsevier) from 2012 to 2017. He has served numerous international conferences as an Organizing Committee Chair, such as IEEE SECON, ICOIN, ICTC, ICUFN, TridentCom, and the IEEE MASS, and as a Program Committee Member, such as IEEE ICC, GLOBECOM, VTC, MobiApps, SENSORNETS, and WINSYS.